Internal Report ITeSRE 291/2000

August 2000

ABSOLUTE TEMPERATURE MEASURES OF THE CMB SPECTRUM: IMPLICATIONS FOR A JOINT ANALYSIS OF ENERGY DISSIPATION PROCESSES AT EARLY AND LATE EPOCHS

C. Burigana and R. Salvaterra

Istituto TeSRE/CNR, via P. Gobetti 101, I-40129 Bologna, Italy

Internal Report ITeSRE 291/2000

August 2000

ABSOLUTE TEMPERATURE MEASURES OF THE CMB SPECTRUM: IMPLICATIONS FOR A JOINT ANALYSIS OF ENERGY DISSIPATION PROCESSES AT EARLY AND LATE EPOCHS

C. Burigana and R. Salvaterra

Istituto TeSRE/CNR, via P. Gobetti 101, I-40129 Bologna, Italy

SUMMARY – In this report we have compared absolute temperature data of the CMB spectrum with models for CMB spectra distorted by a single or two heating processes at different cosmic times. The constraints on the fractional energy injected in the radiation field, $\Delta\epsilon/\epsilon_i$, are mainly provided by the precise measures of the FIRAS instrument aboard the COBE satellite. We find that the baryon density does not influence the limits on $\Delta\epsilon/\epsilon_i$ derived from current data for corresponding cosmic times in terms of the dimensionless time y_h of dissipation epoch, although the redshift corresponding to the same y_h decreases with Ω_b. Under the hypothesis that two heating processes have occurred at different epochs, the former at any y_h in the range $5 \geq y_h \geq 0.01$ (but only for $y_h \gtrsim 0.1$ this analysis results to be meaningful) and the latter at $y_h \ll 1$, the limits on $\Delta\epsilon/\epsilon_i$ are relaxed by a factor ~ 2 both for the earlier and later process with respect to the case in which a single energy injection in the thermal history of the universe is considered. In general, the constraints on $\Delta\epsilon/\epsilon_i$ are weaker for early processes ($5 \gtrsim y_h \gtrsim 1$) than for relatively late processes ($y_h \lesssim 0.1$), because of the sub-cm wavelength coverage of FIRAS data, relatively more sensitive to Comptonization than to Bose-Einstein like distortions.

1 Introduction

As widely discussed in many papers, the spectrum of the Cosmic Microwave Background (CMB) carries unique informations on physical processes occurring during early cosmic epochs (see e.g. Danese & Burigana 1993 and references therein). The comparison between models of CMB spectral distortions and CMB absolute temperature measures can constrain the physical parameters of the considered dissipation processes.

1.1 Theoretical framework

The CMB spectrum emerges from the thermalization redshift, $z_{therm} \sim 10^6 \div 10^7$, with a shape very close to a planckian one, owing to the strict coupling between radiation and matter through Compton scattering and photon production/absorption processes, radiative Compton and Bremsstrahlung, which were extremely efficient at early times and able to re-establish a blackbody (BB) spectrum from a perturbed one on timescales much shorter than the expansion time (e.g. Danese & De Zotti 1977). The value of z_{therm} (Burigana et al. 1991a) depends on the baryon density and the Hubble constant through the product $\widehat{\Omega} = \Omega_b (H_0/50)^2$ (H_0 expressed in Km/s/Mpc).

Physical processes occurring at redshifts $z < z_{therm}$ may lead an imprinting on the CMB spectrum. The CMB distorted spectra depend on at least three main parameters: the fractional amount of energy exchanged between matter and radiation, $\Delta\epsilon/\epsilon_i$, ϵ_i being the radiation energy density before the energy injection, the redshift z_h at which the heating occurs, and the baryon density Ω_b, in units of the critical density.

The analysis of the constraints on the thermal history of the universe set by the high accuracy measurements that have been recently accumulated requires the use of manageable formulae describing spectral distortions for a wide range of the relevant parameters.

The timescale for the achievement of kinetic equilibrium between radiation and matter (i.e. the relaxation time for the photon spectrum), t_C, is

$$t_C = t_{\gamma e} \frac{mc^2}{kT_e} \simeq 4.5 \times 10^{28} \, (T_0/2.7\,K)^{-1} \, \phi^{-1} \widehat{\Omega}_b^{-1} \, (1+z)^{-4} \, \mathrm{sec} \, , \tag{1}$$

where $t_{\gamma e} = 1/(n_e \sigma_T c)$ is the photon–electron collision time, $\phi = (T_e/T_r)$, T_e being the electron temperature and $T_r = T_0(1+z)$; kT_e/mc^2 is the mean fractional change of photon energy in a scattering of cool photons off hot electrons, i.e. $T_e \gg T_r$; T_0 is the present radiation temperature related to the present radiation energy density by $\epsilon_{r0} = aT_0^4$; a primordial helium abundance of 25% by mass is here assumed.

It is useful to introduce the dimensionless time variable $y_e(z)$ defined by

$$y_e(z) = \int_t^{t_0} \frac{dt}{t_C} = \int_1^{1+z} \frac{d(1+z)}{1+z} \frac{t_{exp}}{t_C} \, , \tag{2}$$

where t_0 is the present time and t_{exp} is the expansion time given by

$$t_{exp} \simeq 6.3 \times 10^{19} \left(\frac{T_0}{2.7\,K} \right)^{-2} (1+z)^{-3/2} \left[\kappa(1+z) + (1+z_{eq}) - \left(\frac{\Omega_{nr} - 1}{\Omega_{nr}} \right) \left(\frac{1+z_{eq}}{1+z} \right) \right]^{-1/2} \mathrm{sec} \, , \tag{3}$$

$z_{eq} = 1.0 \times 10^4 (T_0/2.7\,K)^{-4} \widehat{\Omega}_{nr}$ being the redshift of equal non relativistic matter and photon energy densities (Ω_{nr} is the density of non relativistic matter in units of critical density); $\kappa = 1 + N_\nu (7/8)(4/11)^{4/3}$, N_ν being the number of relativistic, 2–component, neutrino species (for

3 species of massless neutrinos, $\kappa \simeq 1.68$), takes into account the contribution of relativistic neutrinos to the dynamics of the universe[1].

Burigana et al. 1991b have reported on numerical solutions of the Kompaneets equation (Kompaneets 1956) for a wide range of values of the relevant parameters.

Under the assumptions of *i*) small distortions, *ii*) dissipative processes with negligible photon production, *iii*) heating close to be instantaneous, a good approximation if the timescale for energy dissipation is much smaller than the expansion timescale, *iv*) distorted radiation spectrum initially represented by a superposition of blackbodies, as is the case for a broad variety of situations of cosmological interest, Burigana et al. 1995 found accurate analytical representations of the numerical solutions for the photon occupation number η computed by Burigana et al. 1991b. They can be expressed in the form

$$\eta = \eta(x; \Delta\epsilon/\epsilon_i, y_h, \widehat{\Omega}_b)\,, \tag{4}$$

where x is the dimensionless frequency $x = h\nu/kT_0$ (ν being the present frequency), and $y_h \equiv y_e(z_h)$ characterizes the epoch when the energy dissipation occurred, z_h being the corresponding redshift (we will refer to $y_h \equiv y_e(z_h)$ computed assuming $\phi = 1$, so that the epoch considered for the energy dissipation does not depend on the amount of released energy).

The form of these analytical approximations is in part suggested by the general properties of the Kompaneets equation and by its well known asymptotic solutions. For $y_h \ll 1$ a superposition of blackbodies is, to a very good approximation, a solution of the Kompaneets equation, except at very low frequencies where photon emission processes are important; when they dominate the Kompaneets equation reduces to an ordinary differential equation. The Comptonization distortion produced by hot gas at small z is a typical example of superposition of blackbodies (Zeldovich & Sunyaev 1969; Zeldovich et al. 1972). At the other extreme ($y_h \gtrsim 5$) the solution is well described by a Bose-Einstein (BE) formula with a frequency dependent chemical potential. For intermediate values of y_h, η has a shape somewhere between these two limiting cases. For $y_h < 1$ the shape of the distorted spectra at long wavelengths is characterized by a minimum of the brightness temperature.

Of course, by combining the approximations describing the distorted spectrum at early and intermediate epochs with the Comptonization distortion expression describing late distortions, we are able to treat two heating processes simultaneously.

1.2 Comparison between observations and models

In this report we compare the recent measures of the CMB absolute temperature with the above models of distorted spectra for one or two heating processes by using a standard χ^2 analysis. The details of our code are described in the Appendix A.

We determine the limits on the amount of energy possibly injected in the cosmic background at arbitrary primordial epochs corresponding to a redshift z_h (or equivalently to y_h). This topic has been discussed in several papers (see e.g. Burigana et al. 1991b, Nordberg & Smoot 1998). We improve here the previous methods of analysis by investigating the possibility of properly combining FIRAS data with longer wavelength measurements and by refining the method of comparison with the theoretical models. We will consider the recent improvement in the calibration of the FIRAS data, that sets the CMB scale temperature at 2.725 ± 0.002 K al 95% CL (Mather et al. 1999). We consider the effect on the estimate

[1] Strictly speaking the present ratio of neutrino to photon energy densities, and hence the value of κ, is itself a function of the amount of energy dissipated. The effect, however, is never very important and is negligible for very small distortions.

of the amount of energy injected in the CMB at a given epoch introduced by the calibration uncertainty of FIRAS scale temperature when FIRAS data are treated jointly to longer wavelength measures. Thus, we are interested to investigate the role of available ground and balloon data compared to the FIRAS measures.

Then, we study the combined effect of two different heating processes that may have distorted the CMB spectrum at different epochs. This hypothesis has been also taken into account by Nordberg & Smoot 1998, who fit the observed data with a spectrum distorted by a single heating at $y_h = 5$, a second one at $y_h \ll 1$ and by free-free emission, obtaining limits on the parameters that describe these processes. We extend their analysis by considering the full range of epochs for the early and intermediate energy injection process, by taking advantage of the analytical representation of spectral distortions at intermediate redshifts (Burigana et al. 1995). Also in this case, the analysis is performed by taking into account the FIRAS calibration uncertainty. We neglect the free-free distortions produced in the case of late dissipation processes in this joint analysis of two heating processes, because the relationship between free-free distortion and Comptonization distortion depends on the details of the thermal history at late epochs (Danese & Burigana 1993, Burigana et al. 1995) and can not simply represented by integral parameters. In addition, free-free distortions are particularly important at very long wavelengths, where the measurements have the largest error bars, at least for energy injection processes which give positive distortion parameters; for cooling processes, which generate negative distortion parameters, the effect may be more relevant also at centimetric wavelengths, but the connection between free-free and Comptonization distortion becames even more critical.

In each case, we fit the CMB spectrum data for three different values (0.01, 0.05 and 0.1) of the baryon density Ω_b. In principle, Ω_b could be constrained by CMB spectrum observations in presence of an early distortion; in this case, a significant change in the χ^2/DOF value for the different choices of this parameter could indicate a favorite value for Ω_b.

Finally, we extend the limits on $\Delta\epsilon/\epsilon_i$ for heatings occurred at $z_h > z_1$, where z_1 is the redshift corresponding to $y_h = 5$, when the Compton scattering was able to restore the kinetic equilibrium between matter and radiation on timescales much shorter than the expansion time and the evolution on the CMB spectrum can be easily studied by replacing the full Kompaneets equation with the differential equations for the evolution of the electron temperature and the chemical potential. This study can be performed by using the simple analytical expressions by Burigana et al. 1991b instead of numerical solutions. For simplicity, we restrict this analysis to the case $\Omega_b = 0.05$ and to the best-fit value of the FIRAS calibration.

2 The data sets

The data reported in Salvaterra & Burigana (2000) are all the measures of the CMB absolute temperature currently available at the different wavelengths. For the present study, we have extracted four different sets of measures, in order to take advantage from the very accurate informations from the FIRAS instrument aboard the COBE satellite. In particular (see Fig. 1), we considered that the statistical error associated to the measure at any channel of FIRAS is very small (0.02÷0.2 mK, Fixsen et al. 1996) and that the scale temperature at which the FIRAS data are set, have a systematic uncertainty of 2 mK at 95% CL given by the calibration uncertainty (Mather et al. 1999). We analyze the impact of the calibration uncertainty in the determination of the amount of the energy injected in the cosmic background, when the FIRAS measures are considered together with the data from ground and balloon experiments. Thus, we combine a collection of recent CMB spectrum data (see Table 1) with the FIRAS data calibrated at the best-fit value as well as at the upper and lower

limit (at 95% CL) of the temperature calibration (see Fig. 2).

In the data files we don't include the measures from the COBRA experiment nor those based on the analysis of the molecular lines, because these experiments fall in the same frequency range of the much more accurate FIRAS measures.

Summing up, we exploit four different data sets:

case 1) The FIRAS data alone; the data reported by Fixsen et al. 1996 are scaled at the most recent calibration value of 2.725 K (Mather et al. 1999) and only the statistical error channel by channel is taken into account. These data are completed by adding four points at 2.735 K (Mather et al. 1990) in the range $1 < \nu < 2$ cm^{-1} with a systematic error of 0.060 K, discarded in the following calibrations of the scale temperature;

case 2) The recent data and the FIRAS data as above, i.e. calibrated at 2.725 K;

case 3) The recent data and the FIRAS data as above but calibrated at 2.723 K (lower calibration limit at 95% CL);

case 4) The recent data and the FIRAS data as above but calibrated at 2.727 K (upper calibration limit at 95% CL).

In this way, we analyze in the last three cases the impact of the FIRAS data calibration in the determination of the amount of the injected energy without losing the important spectral shape informations provided by the small statistical errors in the channel by channel measures.

ν (GHz)	λ (cm)	T_{th} (K)	Error (K)	Reference
0.6	50.0	3.0	1.2	Sironi et al. 1990
0.82	36.6	2.7	1.6	Sironi et al. 1991
1.4	21.3	2.11	0.38	Levin et al. 1988
1.43	21	2.65	$+0.33/-0.30$	Staggs et al. 1996a
1.47	20.4	2.27	0.19	Bensadoun et al. 1993
2	15	2.55	0.14	Bersanelli et al. 1994
2.5	12	2.71	0.21	Sironi et al. 1991
3.8	7.9	2.64	0.06	De Amici et al. 1991
4.75	6.3	2.7	0.07	Mandolesi et al. 1986
7.5	4.0	2.6	0.07	Kogut et al. 1990
7.5	4.0	2.64	0.06	Levin et al. 1992
10	3	2.62	0.058	Kogut et al. 1988
10.7	2.8	2.730	0.014	Staggs et al. 1996b
24.8	1.2	2.783	0.089	Johnson & Wilkinson 1987
33	0.909	2.81	0.12	De Amici et al. 1985
90	0.33	2.60	0.09	Bersanelli et al. 1989
90	0.33	2.712	0.020	Schuster et al.

Table 1: Values of the recent measures of the absolute thermodynamic temperature of CMB spectrum.

3 Fit results

The fits are based on the χ^2 analysis, carried out with a specific program, MINPUZZLE, based on the MINUIT package of the CERN library and on the collection of subroutines

and functions, PUZZLE, developed by C. Burigana in the 1994, that implements the semi-analytical description of the CMB distorted spectra (Burigana et al. 1995). This program allows to compare the CMB distorted spectrum models with the observational data without the necessity of interpolating frames of numerical solutions (as in Burigana et al. 1991b) to make the computation much more faster without any significant loss of accuracy, given the very good agreement between the semi-analytical expressions and the numerical solutions.

The CMB spectrum data are compared with the models by the minimization routines SIMPLEX and MIGRAD (see Appendix A and the MINUITS/CERN documentation for further details). The physical parameters that describe the distorted spectrum, can be set by the user choosing on which ones to have the fit. A more detailed description of the inputs and the outputs of the program is also provided in Appendix A.

The main goal is to obtain informations on the value of the CMB absolute temperature and the energy injected in the cosmic background, $\Delta\epsilon/\epsilon_i$, from the different data sets. The data sets are fitted with the distorted spectrum for different values of the dimensionless time parameter y_h ($y_h = 5$, 4, 3, 2, 1, 0.5, 0.25, 0.1, 0.05, 0.025, 0.01 and $\ll 1$) in order to determine the value and the relative uncertainty of the energy injected at the corresponding epoch. In APPENDIX B, Tab. 8, we provide the values of z_h corresponding to y_h for the considered values of Ω_b; note how the redshift z_h corresponding to a given value of y_h decreases with the increase of baryon density. All the plots of these fits are reported in Appendix B.

3.1 Fits with a single energy injection

In this section we present the results of the fit of the four data sets described in §2 with spectra distorted by a single energy injection.

The results obtained for the *case* 1) (FIRAS data only) are shown in Fig.s 3-4 for the full set of y_h and the representative case $\Omega_b = 0.05$; in Fig.s 16-17 (Appendix B) we report the results for the three choices of Ω_b.

The results are always compatible with null values of the distortion parameters, the best fit values of $\Delta\epsilon/\epsilon_i$ being only just different from zero. The χ^2 best fit value does not change significantly with y_h and Ω_b, being the χ^2/DOF very close to unit; this means that this data do not allow to indicate a favourite epoch for a possible (very small) energy injection nor provide informations on the baryon density. On the other hand, the limits on $\Delta\epsilon/\epsilon_i$ significantly depend on the epoch of the energy injection, being about a factor two larger for early than for late dissipation processes; this is clearly related to the range of frequencies observed by FIRAS.

In principle, the measures at centimetric and decimetric wavelengths could play a crucial role to investigate on the presence of early distortions, due to the large decrease of the CMB absolute temperature in the Rayleigh-Jeans region. The results found for the *case* 2) (recent data and FIRAS data calibrated at 2.725 K) and $\Omega_b = 0.05$ are shown in Fig.s 5 and 6, whereas the in Fig.s 18 and 19 (Appendix B) we exploit the three choices of Ω_b. As evident from the comparison with the results of the *case* 1), the ground and balloon data do not change significantly the contraints on energy dissipations with respect to the FIRAS measures alone, independently of the considered energy injection epoch, because of the corresponding large error bars.

Even considering the full range of frequecies, it is impossible to determine a favourite energy injection epoch or a favourite baryon density value, as indicated by the χ^2 values, substantially constant with y_h and Ω_b. The χ^2/DOF (~ 1.1) is only just larger than that obtained in the *case* 1). This weak increae is due to the well known disagreement between the absolute temperature of the FIRAS data and the averaged temperature of the data at $\lambda > 1$ cm.

For sake of completeness, we have analyzed the impact of the uncertainty of 2 mK (at 95% CL, Mather et al. 1999) in the FIRAS data calibration when they are combined with the recent measures at longer wavelenghts (see the figures reported in APPENDIX B). In the *case* 3) (FIRAS data calibrated at 2.723 K, see Fig.s 20 and 21) and in the *case* 4) (FIRAS data calibrated at 2.727 K, see Fig.s 22 and 23) we find that the systematic uncertainty in the FIRAS calibration does not have any significant impact on the fits results. By assuming the lowest FIRAS calibration only a small improvement of $\sim 2\%$ in the χ^2/DOF is found with respect to the case of the highest calibration, as expected since the lower averaged temperature value at $\lambda > 1$ cm than at $\lambda < 1$ cm.

Thus, our analysis demonstrate that the current contraints on the energy possibly injected in the cosmic radiation field are essentially set by the FIRAS measures alone independently of the cosmic epoch.

No significant informations on Ω_b or on the epoch of a possible energy injection can be currently obtained because of the spectral shape of FIRAS data, so close to a planckian spectrum.

Finally, we report in Tab.s 2-4 the values of best-fit of the fractional injected energy, $\Delta\epsilon/\epsilon_i$, in the case of a heating process at early ($y_h = 5$, BE like spectrum) and late ($y_h \ll 1$, Comptonizated spectrum) epochs, with the corresponding uncertainties at 95% CL

3.2 Fits with two energy injections

We quantify here the constraints set by the available measures when we take into account the possibility that two heating processes could have distorted the CMB spectrum at different epochs, early or intermediate for the former and late for the latter. More explicitely, we obtain the limits on the amount of the first energy injection for each value of y_h (in the range $5 \geq y_h \geq 0.01$) under the hypothesis of a possible existence of a second late heating (at $y_h \ll 1$) and on the amount of the second late energy injection (at $y_h \ll 1$) under the hypothesis of a possible existence of an earlier energy dissipation occuring at different values of y_h (in the range $5 \geq y_h \geq 0.01$).

In this analysis we use again the semi-analytical description of the distorted spectra at $5 \gtrsim y_h \gtrsim 0.01$ (Burigana et al. 1995) and take advantage from the possibility of our code to semi-analytically describe the combined effect of early, intermediate and late distortions (see Appendix A).

So far, we extend the analysis of Nordberg & Smoot 1998 which considered only the case of an early dissipation at $y_h = 5$ combined with a late one at $y_h \ll 1$. Our results are then clearly comparable to those obtained in the previous section: we expect that, by including the possibility of two heating processes at different cosmic epochs, the constraints on $\Delta\epsilon/\epsilon_i$, both for early and late processes, are relaxed with respect to the case in which a single heating in the thermal history of the universe is considered.

For this purpose we exploit the whole frequency range of CMB spectrum measures [i.e. the data sets corresponding to *case* 2), *case* 3), and *case* 4)].

The results of this analysis are again fully reported in APPENDIX B (Fig.s 24-32) and are organized in three set of plots.

The first set of plots [see Fig. 24 for the *case* 2), Fig. 27 for the *case* 3), and Fig. 30 for the *case* 4)] shows the best fit value of the energy injected at a certain value of y_h and its relative upper and lower limits at 95% CL when we allow for a second heating will have occurred at $y_h \ll 1$.

The second set of plots [see Fig. 25 for the *case* 2), Fig. 28 for the *case* 3), and Fig. 31 for the *case* 4)] reports the best fit value of the energy injected at $y_h \ll 1$ and its upper and lower limits when we allow for an earlier energy dissipation occurring at a certain epoch y_h.

Data set	$(\Delta\epsilon/\epsilon_i)/10^{-5}$	
	heating at $y_h = 5$	heating at $y_h \ll 1$
FIRAS	0.23 ± 5.33	0.28 ± 2.33
recent and FIRAS (2.725 K)	0.63 ± 5.32	0.28 ± 2.33
recent and FIRAS (2.723 K)	$0.63^{+5.34}_{-5.33}$	0.29 ± 2.34
recent and FIRAS (2.727 K)	0.66 ± 5.31	0.29 ± 2.33

Table 2: Results on the injected energy at $y_h = 5$ and at $y_h \ll 1$ by assuming $\Omega_b = 0.01$. Fits to the different data sets, errors at 95% CL.

Data set	$(\Delta\epsilon/\epsilon_i)/10^{-5}$	
	heating at $y_h = 5$	heating at $y_h \ll 1$
FIRAS	$0.23^{+5.33}_{-5.32}$	0.28 ± 2.33
recent and FIRAS (2.725 K)	$0.64^{+5.32}_{-5.31}$	0.28 ± 2.33
recent and FIRAS (2.723 K)	0.63 ± 5.33	0.29 ± 2.34
recent and FIRAS (2.727 K)	$0.66^{+5.31}_{-5.30}$	0.29 ± 2.33

Table 3: The same as in Tab. 2 but for $\Omega_b = 0.05$.

Data set	$(\Delta\epsilon/\epsilon_i)/10^{-5}$	
	heating at $y_h = 5$	heating at $y_h \ll 1$
FIRAS	$0.23^{+5.33}_{-5.32}$	0.28 ± 2.33
recent and FIRAS (2.725 K)	0.61 ± 5.32	0.28 ± 2.33
recent and FIRAS (2.723 K)	$0.61^{+5.34}_{-5.33}$	0.29 ± 2.34
recent and FIRAS (2.727 K)	0.64 ± 5.31	0.29 ± 2.33

Table 4: The same as in Tab. 2 but for $\Omega_b = 0.1$.

The third set of plots (see Fig. 26 for the *case* 2), Fig. 29 for the *case* 3), and Fig. 32 for the *case* 42)] gives the χ^2/DOF corresponding to the models with the best fit values obtained by allowing for a late dissipation and an earlier dissipation at a certain epoch y_h.

In each figure we show our results for the three considered values of Ω_b.

The results obtained in the *case* 2) for $\Omega_b = 0.05$ are also reported in Fig.s 7-9.

We note here that, in general, the jointly analysis of two dissipation processes results to be meaningless for the earlier processes occurring at $y_h < 0.1$, when the limits on the amount of injected energy became very relaxed. This is due to the fact that the imprints produced by a positive (negative) distortion at any $y_h < 0.1$ can be compensated by those produced by a negative (positive) at $y_h \ll 1$.

As shown by the values reported in Tab.s 5-7 for the case of a joint analysis of an heating at $y_h = 5$ and one at $y_h \ll 1$, the limits on $\Delta\epsilon/\epsilon_i$ are relaxed by a factor ~ 2 with respect to the case of in which a single energy injection in the thermal history is considered, both for early and late dissipation processes (for comparison see Tab.s 2-4).

Different FIRAS calibrations do not introduce significant differences in the fit results; again, the exact FIRAS calibration returns to be not crucial in the exploitation of current data.

Finally, the χ^2 value is substantially constant for the different values of y_h and Ω_b.

4 Constraints on energy injections at very high redshifts

For $z > z_1$ (i.e. $y_h > 5$) the Compton scattering is able, after an energy injection, to restore the kinetic equilibrium between matter and radiation yielding a BE spectrum on timescales smaller than the expansion time, while radiative Compton and Bremsstrahlung work to restore the thermodynamic equilibrium yielding a BB spectrum. Thus, a bigger amount of energy would have been needed to yield the same observed effect produced by a dissipation processes at $\sim z_1$. The analytic approximations of Burigana et al. 1991b of the numerical computations carried out by Burigana et al. 1991a,b permits us to extend the limits on $\Delta\epsilon/\epsilon_i$ at $z_h > z_1$ with good accuracy without the necessity of numerical integrations of the chemical potential and electron temperature evolution equations. We have considered here only the case with $\Omega_b = 0.05$, for simplicity.

We extend at high z the limits on $\Delta\epsilon/\epsilon_i$ at 95% CL obtained from the accurate measures of FIRAS data alone [*case* 1)] and from the recent measures from ground and balloon combined with the FIRAS data calibrated at 2.725 K [*case* 2)]. The results, plotted in Fig.s 10 and 11, are very close one each other, in strict analogy with the corresponding limits on the amount of energy injected at $z = z_1$. The limits set by the FIRAS data significantly constrain the value of $\Delta\epsilon/\epsilon_i$ also at $z > z_1$; of course, they can not exclude that a very large amount of energy could have been dissipated at $z \approx z_{therm}$. At $z > z_{therm}$ limits on the energy possibly injected in the radiation field can be set by primordial nucleosynthesis analyses.

We obtain also the limits on $\Delta\epsilon/\epsilon_i$ at high z by allowing for a second heating will have occurred at low z (see Fig. 12). In this case, the limits at 95% CL on the amount of the energy injected at $z = z_1$, relaxed compared to the case of a single heating in the thermal history of the universe, allow for larger energy dissipations (up to a factor ~ 2), particularly at $z_1 \lesssim z \lesssim z_{therm}/2$.

5 Conclusions

In this report we have compared absolute temperature data of the CMB spectrum with models for CMB spectra distorted by a single or two heating processes at different cosmic

Data set	$(\Delta\epsilon/\epsilon_i)/10^{-5}$	
	heating at $y_h = 5$	heating at $y_h \ll 1$
recent and FIRAS (2.725 K)	$0.36^{+9.63}_{-9.62}$	0.14 ± 4.17
recent and FIRAS (2.723 K)	$0.26^{+9.67}_{-9.66}$	0.19 ± 4.19
recent and FIRAS (2.727 K)	$0.41^{+9.62}_{-9.60}$	0.13 ± 4.17

Table 5: Results on the energy injected at $y_h = 5$ and $y_h \ll 1$ when these two dissipation processes are jointly considered. Fits to the different data sets assuming with $\Omega_b = 0.01$; errors at 95% CL.

Data set	$(\Delta\epsilon/\epsilon_i)/10^{-5}$	
	heating at $y_h = 5$	heating at $y_h \ll 1$
recent and FIRAS (2.725 K)	$0.37^{+9.62}_{-9.61}$	0.14 ± 4.17
recent and FIRAS (2.723 K)	$0.27^{+9.66}_{-9.64}$	0.19 ± 4.19
recent and FIRAS (2.727 K)	$0.42^{+9.61}_{-9.61}$	$0.12^{+4.16}_{-4.17}$

Table 6: The same as in Tab. 5 but for $\Omega_b = 0.05$.

Data set	$(\Delta\epsilon/\epsilon_i)/10^{-5}$	
	heating at $y_h = 5$	heating at $y_h \ll 1$
recent and FIRAS (2.725 K)	$0.29^{+9.64}_{-9.62}$	0.17 ± 4.17
recent and FIRAS (2.723 K)	$0.19^{+9.67}_{-9.66}$	0.21 ± 4.19
recent and FIRAS (2.727 K)	$0.34^{+9.62}_{-9.60}$	0.15 ± 4.17

Table 7: The same as in Tab. 5 but for $\Omega_b = 0.1$.

times.

We have computed the limits on the amount of the energy injected in the radiation field for the whole range of cosmic epochs, expressed here in terms of the dimensionless time variable y_h. These upper and lower limits on $\Delta\epsilon/\epsilon_i$ are mainly provided by the precise measures of the FIRAS instrument aboard the COBE satellite; the addition of the data obtained from ground and balloon experiments at higher wavelengths does not alter significantly the results based on the FIRAS data alone, because of the large error bars of the measures at $\lambda \gtrsim 1$ cm. We analyzed also the impact of the FIRAS calibration on the determination of $\Delta\epsilon/\epsilon_i$ when the FIRAS data are used together with the ground and balloon measures: the uncertainty of 2 mK at 95% CL in the FIRAS calibration (Mather et al. 1999) doesn't affect significantly the limits on $\Delta\epsilon/\epsilon_i$. From the χ^2 analysis it results weakly favoured the lower limit at 2.723 K. This is due to the well known disagreement of absolute temperature of the FIRAS data and of the mean temperature of the data at $\lambda > 1$ cm.

We considered different values of the baryon density, i.e. of Ω_b. For the same y_h, the value of this parameter does not influence the upper and lower limits on the amount of the injected energy (of course, $z_h(y_h)$ decreases with Ω_b).

As in the case of a single heating, we exploit the CMB spectrum data under the hypothesis that two heating processes have occurred at different epochs, the former at any y_h in the range $5 \geq y_h \geq 0.01$ (but only for $y_h \gtrsim 0.1$ this analysis results to be meaningful) and the latter at $y_h \ll 1$. The limits on $\Delta\epsilon/\epsilon_i$ are relaxed by a factor ~ 2 both for the earlier and later process with respect to the case in which a single energy injection in the thermal history of the universe is considered.

Also in this case, we analyzed the impact of the FIRAS calibration and the role of the baryon density. The results are very similar to those obtained for the case of single heating.

In general, the constraints on $\Delta\epsilon/\epsilon_i$ are weaker for early processes ($5 \gtrsim y_h \gtrsim 1$) than for relatively late processes ($y_h \lesssim 0.1$), because of the sub-cm wavelength coverage of FIRAS data, relatively more sensitive to Comptonization than to Bose-Einstein like distortions.

Finally, we evaluate the limits on $\Delta\epsilon/\epsilon_i$ for energy injections occuring during the kinetic equilibrium period (i.e. at $z \gtrsim z_1$) by allowing also for a further late dissipation process, in which case the constraints on $\Delta\epsilon/\epsilon_i$ return to be relaxed (up to a factor ~ 2) with respect to the case of a single injection at high z, particularly at $z_1 \lesssim z \lesssim z_{therm}/2$.

In conclusion, the available data permit to set very stringent constraints on the energy injected in the radiation field at different cosmic times, mainly set by the precise measures of FIRAS. The role of future more precise measurements at $\lambda > 1$ cm, particularly significant for early dissipation processes, will be discussed in a forthcoming work.

Acknowledgements. It is a pleasure to thank M. Bersanelli, L. Danese, G. De Zotti, N. Mandolesi and G. Palumbo for useful and stimulating discussions.

Figure 1: Comparison between the FIRAS data reported by Mather et al. 1994 and the more refined analysis by Fixsen et al. 1996, that allow to significantly reduce the statistical error of each frequency channel. The absolute calibration of 2.726 K by Mather et al. 1994 changed to 2.728 K in the Fixsen et al. 1996 revision and finally to 2.725 K $\pm$ 0.002 K (95% CL) in the re-analysis of Mather et al. 1999.

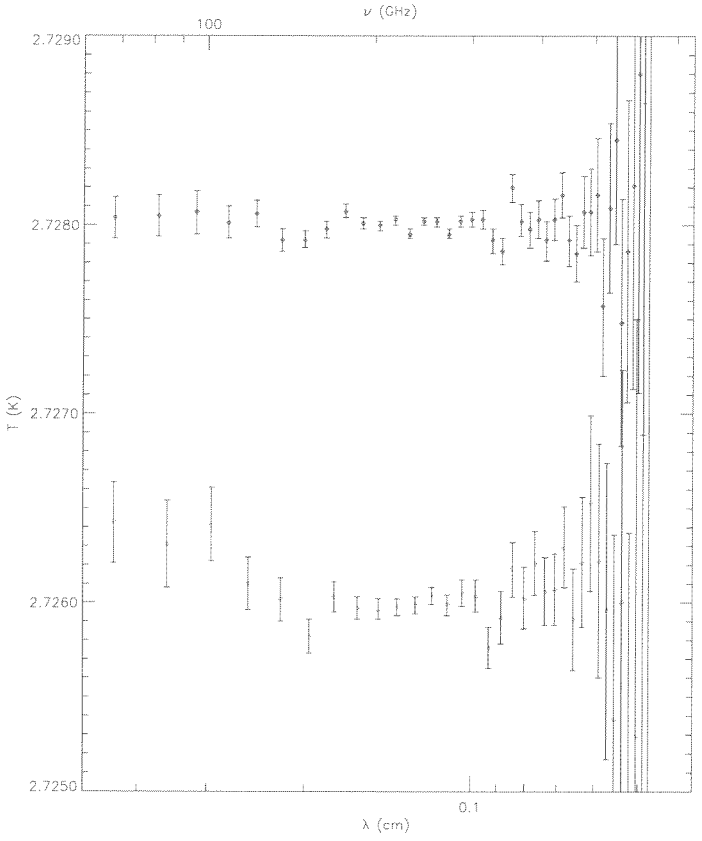

Figure 2: Longwavelength measures of the CMB spectrum (see Table 1) compared to the FIRAS data reported here with simple lines (see also the text for further details).

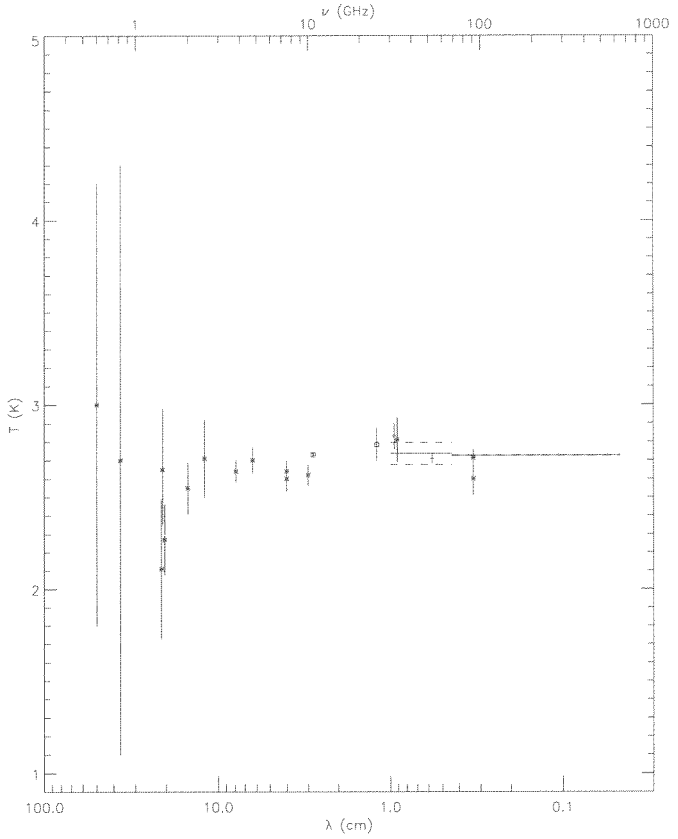

Figure 3: Values of the fractional energy injected in the radiation field as obtained from the fit to the FIRAS data alone. The solid line represents the best-fit, the dashed lines are the upper and the lower limits at 95% CL.

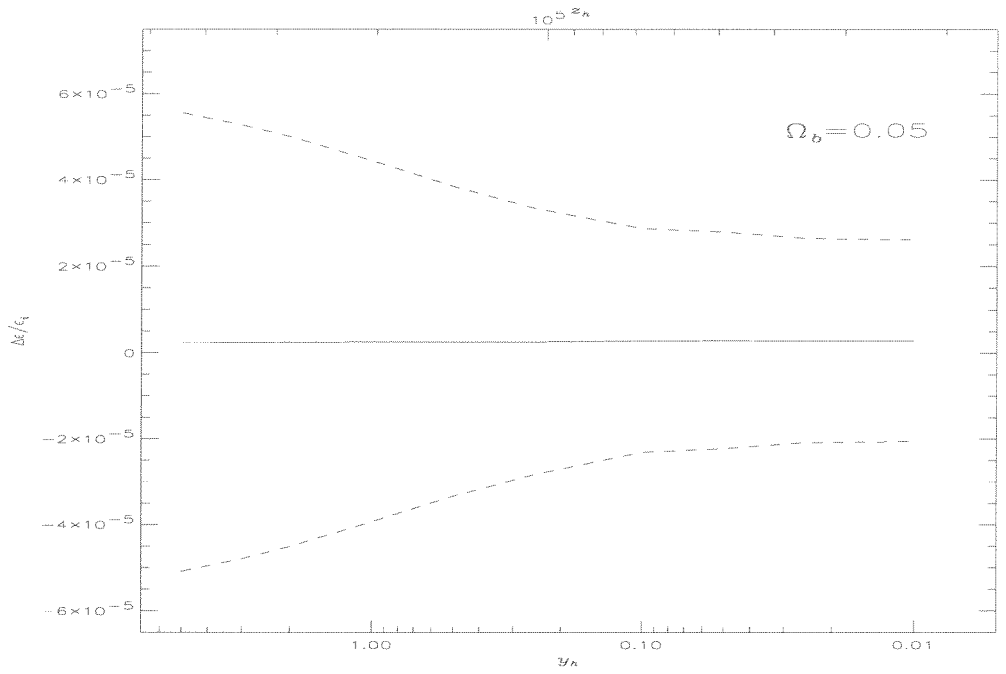

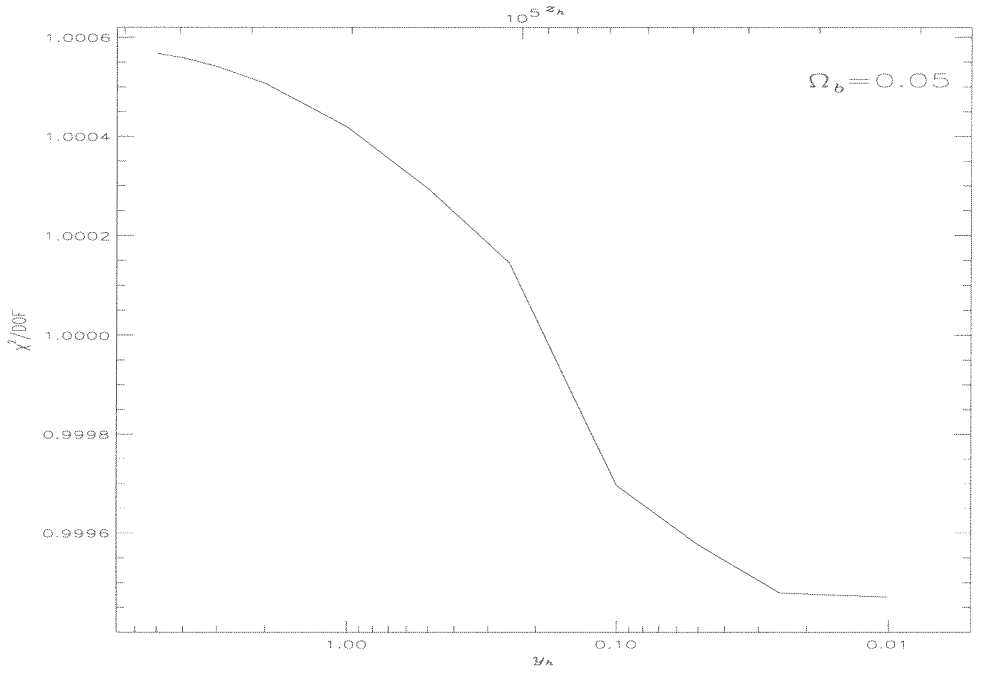

Figure 4: Values of χ^2/DOF for the fit to the FIRAS data. We fit 47 data with 2 parameters: T_0 and $\Delta\epsilon/\epsilon_i$.

Figure 5: Values of the fractional energy injected in the radiation field as obtained from the fit to the recent data jointed to the FIRAS data calibrated at 2.725 K. The solid line is the best-fit, the dashed lines are the upper and the lower limits at 95% CL.

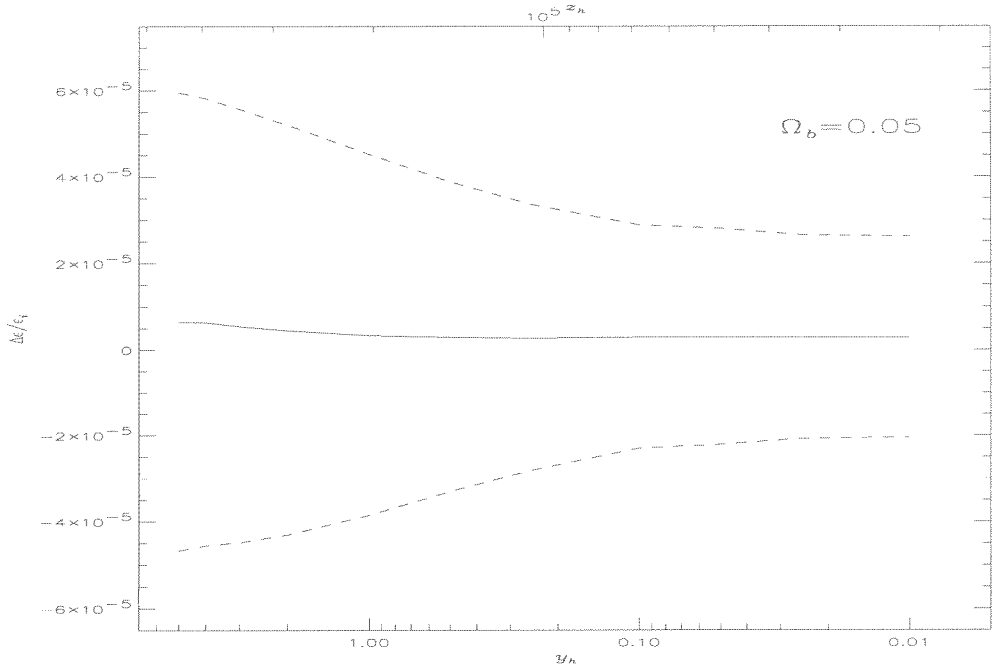

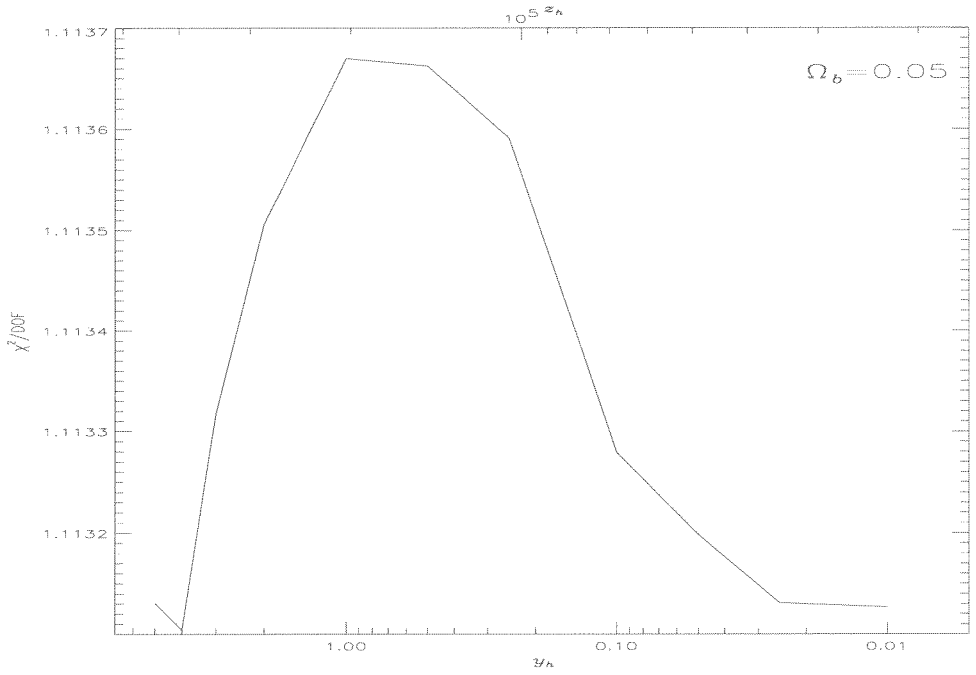

Figure 6: Values of χ^2/DOF for the fit to the recent data jointed to the FIRAS data calibrated at 2.725 K. We fit 64 data with 2 parameters: T_0 and $\Delta\epsilon/\epsilon_i$.

Figure 7: Results of the fit on the energy injected at any given value of y_h and relative upper and lower limits at 95% CL by allowing also for a dissipation process at low z. We used here the recent data jointed to the FIRAS data calibrated at 2.725 K.

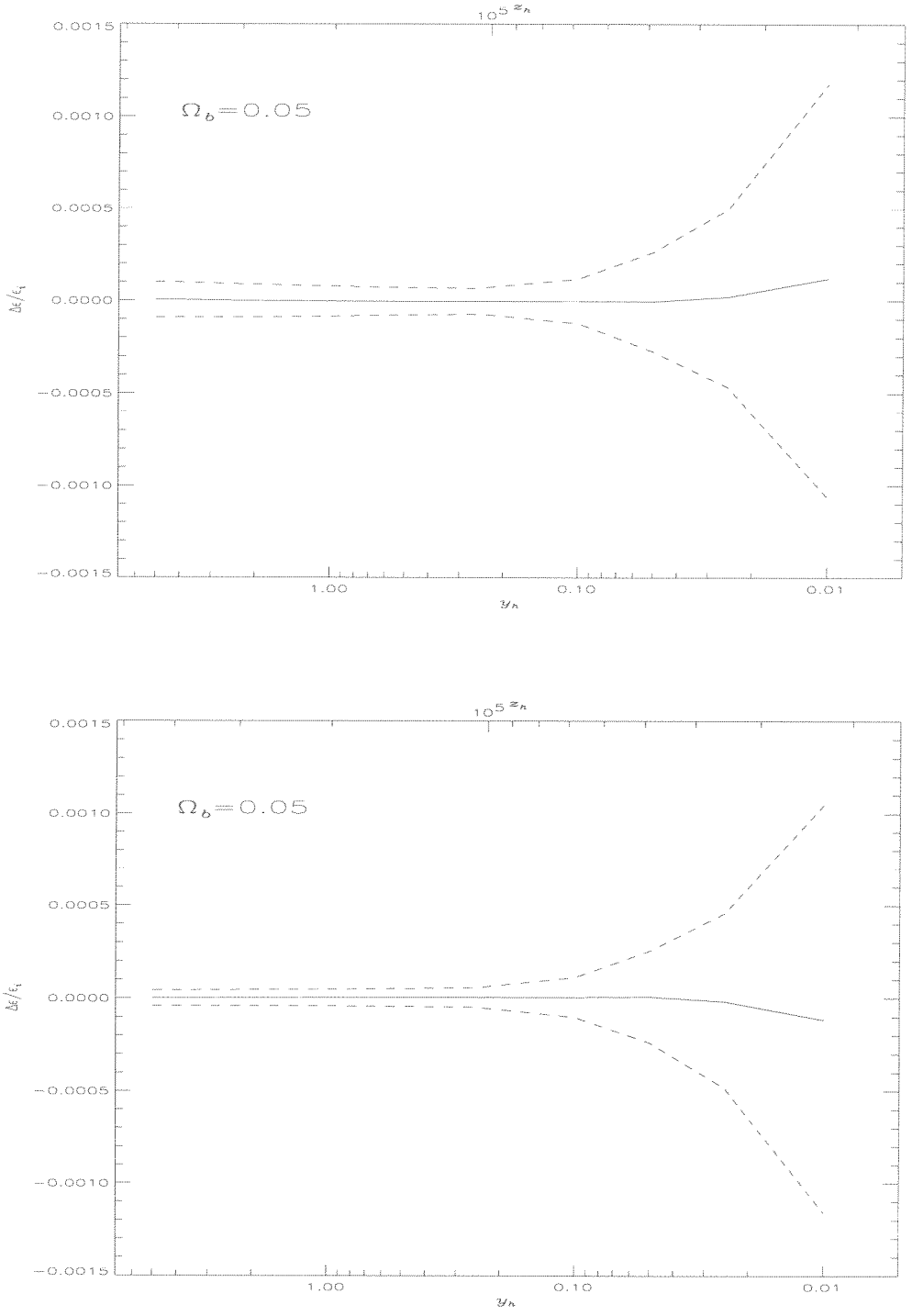

Figure 8: Results of the fit on the energy injected at low z and relative upper and lower limits at 95% CL by allowing also for a previous energy dissipation occurring at a given y_h. We used here the recent data jointed to the FIRAS data calibrated at 2.725 K.

Figure 9: Values of the χ^2/DOF of the fit to the recent data jointed to the FIRAS data calibrated at 2.725 K. We fit 64 data with 3 parameters: T_0 and two values of $\Delta\epsilon/\epsilon_i$ corresponding to two dissipation processes at different epochs.

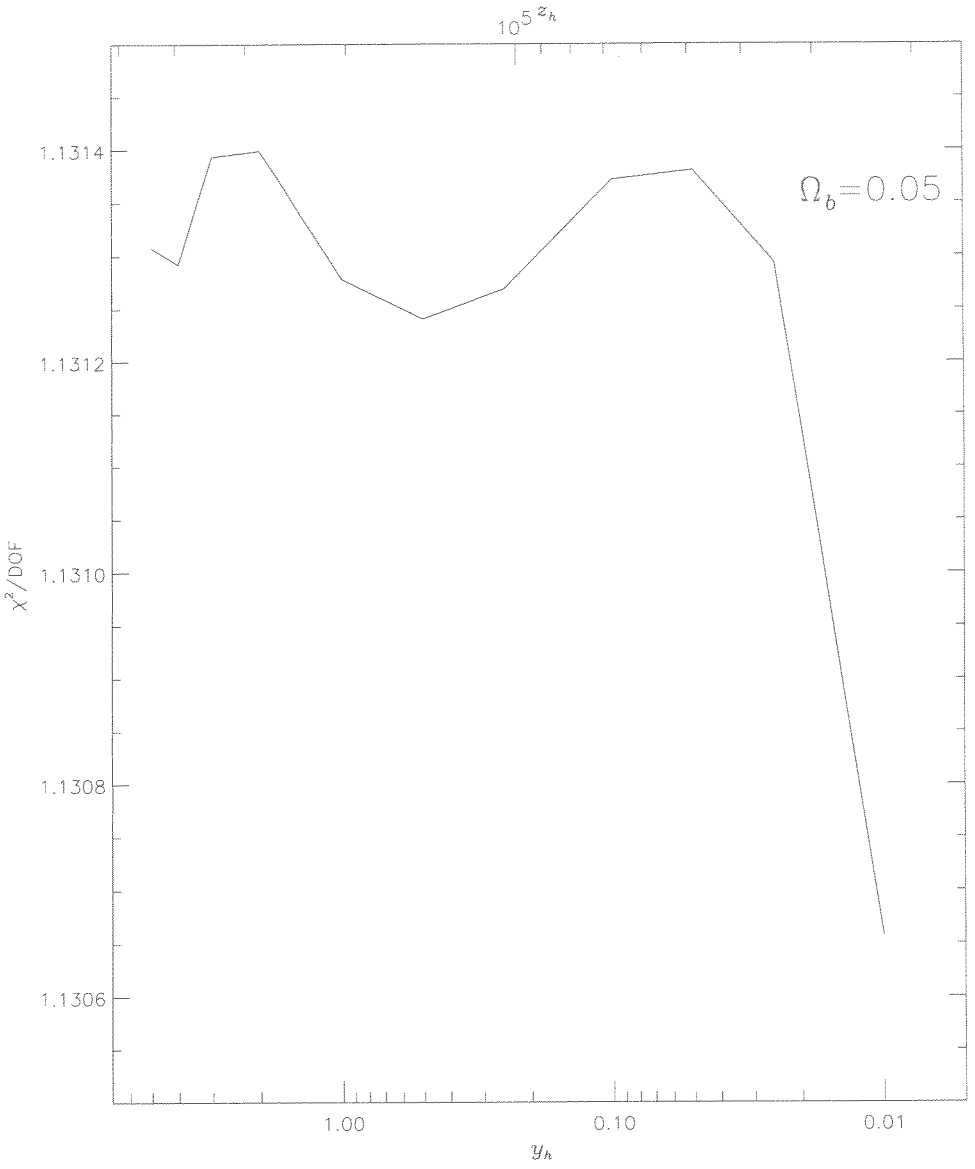

Figure 10: Extension of the upper (top panel) and the lower (bottom panel) limits at 95% CL on the amount of the energy injected at $z_1 \leq z_h < 0.9 z_{therm}$ obtained with the FIRAS data alone ($\Omega_b = 0.05$).

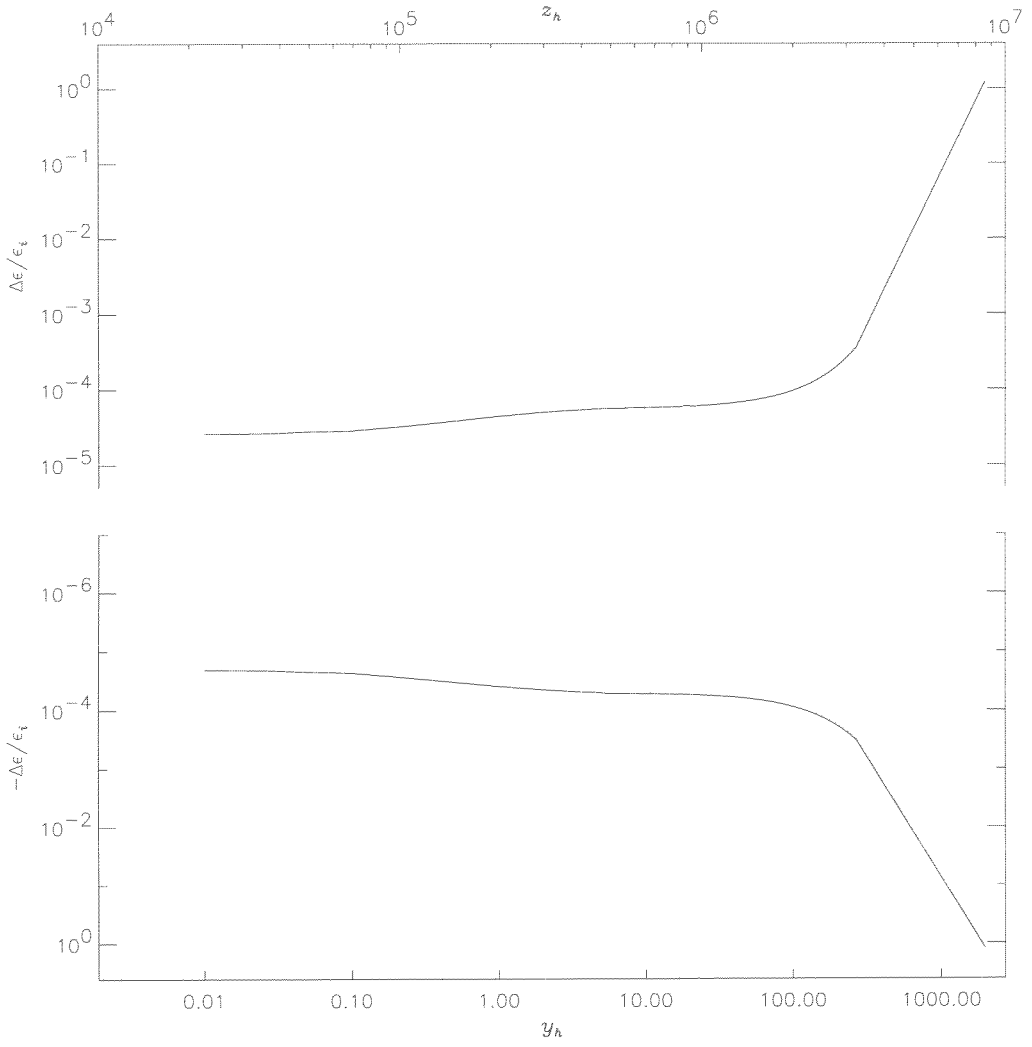

Figure 11: Extension of the upper (top panel) and the lower (bottom panel) limits at 95% CL on the amount of the energy injected at $z_1 \leq z_h < 0.9 z_{therm}$ obtained with the recent data from ground and balloon jointed to the FIRAS data ($\Omega_b = 0.05$).

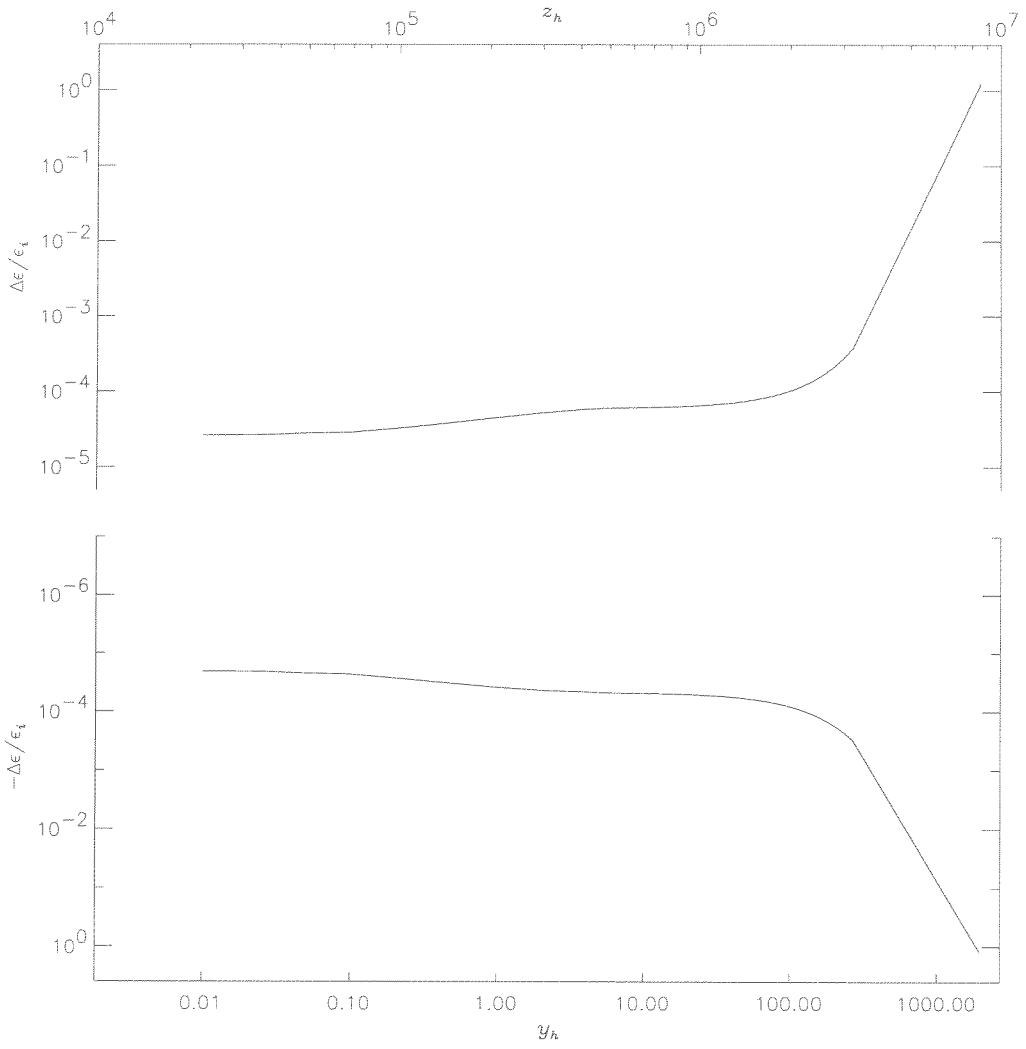

Figure 12: Extension of the upper (top panel) and the lower (bottom panel) limits at 95% CL on the amount of the energy injected at $z_1 \leq z_h < 0.9 z_{therm}$ obtained with the recent data from ground and balloon and the FIRAS data by allowing for a late dissipation process ($\Omega_b = 0.05$).

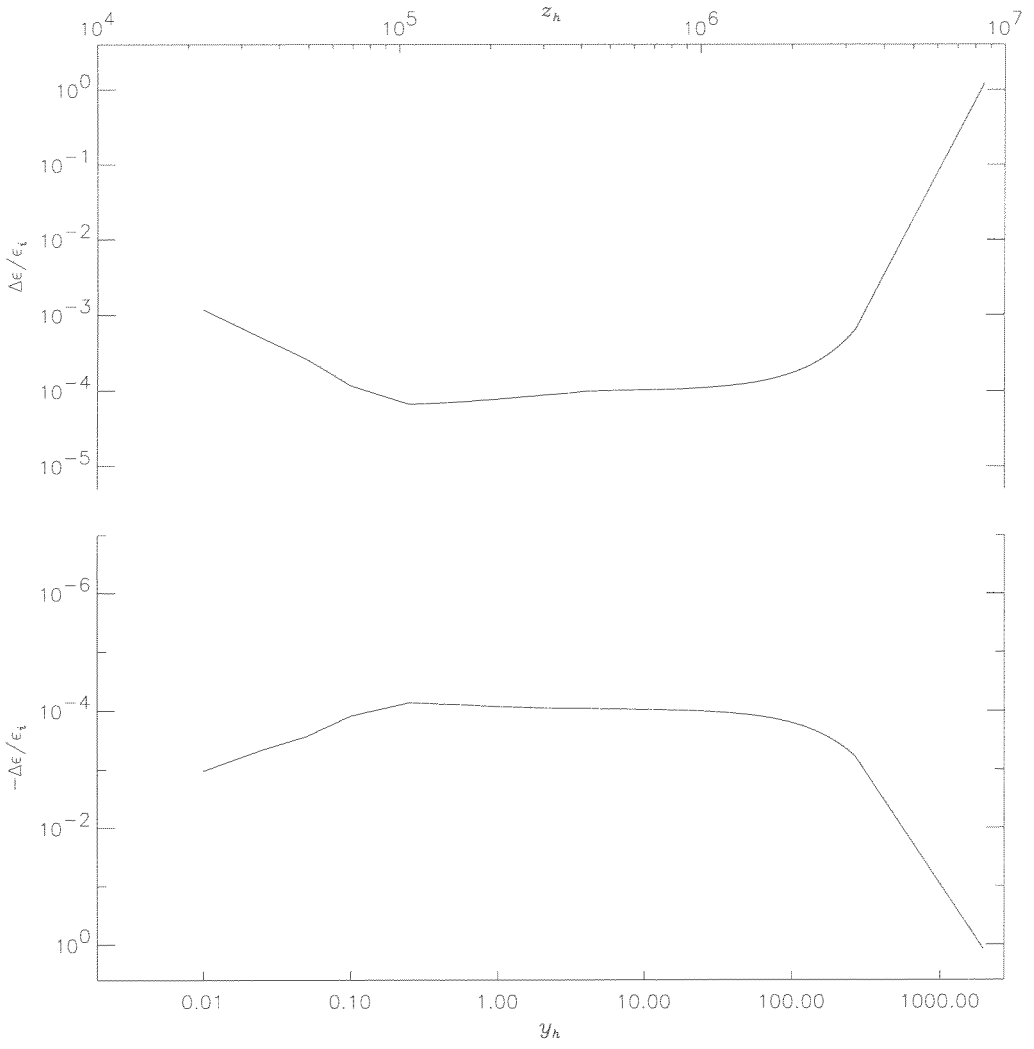

A Brief description of the code to fit CMB spectrum data

We have written a FORTRAN code, MINPUZZLE, to fit the CMB spectrum observations with theoretical models through the minimization package, MINUITS, of the CERN library (http://cern.web.cern,ch/CERN/). The code which describes the theoretical models, PUZZLE, is the collection of subroutines and functions developed by C. Burigana in the 1994 that implements the semi-analytical description of the CMB distorted spectrum reported by Burigana et al. 1995. The distorted spectrum is compared with the observational data through the χ^2 analysis without the necessity of interpolating extensive numerical solutions as in Burigana et al. 1991b. The code is then much more faster without loss of informations, since the very good the agreement between semi-analytical formulae and numerical solutions. See the Sect. 6 of Burigana et al. 1995 for a description of the logical procedure to compute the distorted spectrum for any choice of the relevant parameters taking advantage of the semi-analytical approximations described there.

The program MINPUZZLE allows to control through an input file of parameters both the desired fit functions of the MINUITS package and the values of the physical parameters needed to compute the distorted spectrum. The independence of this file from the main program permits to change its contents without altering the main program.

Fig. 13 shows a typical example of this input file. The first 15 lines introduce the values of the physical parameters necessary to compute the distorted spectrum. Each parameter can be also declared FIX and in this case its value is fixed to the value set by the user and the program does not carry out the fit on this parameter. A number (first column) and a name between apices (second column) is assigned to each parameter. The meaning of these names is reported here below:

1. 'dT0' = $dT_0 = T_{fit} - T_0$ is the difference between the temperature T_0 as calculated in the fit, T_{fit}, and the expected temperature, T_0. In this way, we can appreciate the small differences in the best-fit temperature obtained by exploiting the different data sets;

2. 'mu' = μ_0 is a parameter characterizing the distortion occurred at high and intermediate z related to the fractional injected energy through $\mu_0 = 1.4\Delta\epsilon/\epsilon_i$ (only the case of small distortions is relevant in the comparison with the data);

3. 'uheat0' = u is the value of the Comptonization parameter of the distortion occurred at low z (i.e. at $y_h \ll 1$): $u = 1/4\Delta\epsilon/\epsilon_i$ (again, only the case of small distortions is relevant in the comparison with the data);

4. 'yB0=$y_{B,0}$' is the parameter characterizing the free-free distortion, analogous to 'uheat0'.

5. 'history' identifies several kinds of simple thermal histories, subsequent to those described by the parameters of the previous points 2. $\div$ 5., according to some flag values. We remember that a proper joint analysis of Comptonization and free-free distortions requires to model the thermal history of the universe. If 'history' = -10 we have the trivial case in which $\phi = \phi_{in}$ between z_{start} and z_{end}, i.e. we have thermal equilibrium and the Comptonization and free-free parameters do not grow with respect to uheat0 and yB0. If 'history' = 0 we have a thermal history with $\phi = \mathrm{cost} = \phi_0$, if 'history' = 1 with $\phi = \phi_0(1+z)^n$, if 'history' = -1 with $T_e = \mathrm{cost} = T_{e,0}$ (i.e. $\phi_0 = T_{e,0}/T_0$) and if 'history' = 10 with $\phi_0 = \phi_{start} + (\phi_{end} - \phi_{start})/(\ln(1+z_{end}) - \ln(1+z_{start}))(\ln(1+z) - \ln(1+z_{start}))$. In this work 'history' is always fixed to -10;

6. 'nfi' = is the exponent n in the case of a thermal history represented by a power law, so that $\phi = \phi_0(1+z)^n$ (the case with 'history' = 1;

7. 'Fi0' = ϕ_0; input parameter for the cases 'history' = 0 and 1;

8. 'Te0' = $T_{e,0}$ represent the case T_e = cost = $T_{e,0}$ equivalent to $\phi_0 = T_{e,0}/T_0$, necessary in the case 'history' = −1;

9. 'zstart' = z_{start} is the redshift at which the heating starts;

10. 'zend' = z_{end} is the redshift at which the heating ends;

11. 'omegab' = Ω_b give the baryon density in units of critical density;

12. 'rH50' = H_0 in units of 50 Km/s/Mpc;

13. 'omegaNR' = Ω_{NR} give the non relativistic matter density in units of critical density;

14. 'kn' = k_n is the parameter that takes into account the number of relativistic, 2-component, massless, neutrino species ('kn' = 1.681322 for 3 species).

In the third column the user fixes the value of the considered parameter or indicates the starting value when the fit on this parameter will be performed. In this case may be necessary to set also an indicative (upper) error with which the best-fit is wanted (4th column) and the physical limits (5th and 6th column) on this parameter. If the fit obtains results outside this range, the program will report that the minimum is outside the range of the acceptable values.

The user has to set the orders needed to make the fit. First, the confidence level of the result on a parameter when the other parameters are free (ERROR DEF) is to be set. The value 4 indicates the 95% CL. Moreover, the user has to set the routines of the MINUITS package to use. In our case, the routines MINIMIZE and MINOS are used.

The MINIMIZE command calls MIGRAD to compute the minimum and the error matrix. Unlike the simple MIGRAD command MINIMIZE reverts to SIMPLEX, if MIGRAD fails, and then calls MIGRAD again. MIGRAD is the best minimizer of the package for nearly all functions. Its main weakness is that it depends heavily on knowledge of the first derivatives, and fails miserably if they are very inaccurate. The SIMPLEX routine is usually much slowly than MIGRAD, but it does not use first derivates, so it should not be so sensitive to the precision of the χ^2 calculations. It gives no reliable information about parameter errors, no information about parameter correlations, and worst of all cannot be expected to converge accurately to the minimum in a finite time. An example of the output of MINIMIZE is given in Fig. 14.

MINOS calculates the parameter errors taking into account both parameter correlations and non-linearities. MINOS can only operate after a good minimum has already been found, and the error matrix has been calculated, so the MINOS command will normally follow a MIGRAD command. The MINOS error for a given parameter is defined as the change in the value of that parameter which causes the χ^2 to increase by the amount UP, where UP is the ERROR DEF value specified by the user. The algorithm to find the positive and negative MINOS error for the n-th parameter consists of varying n-th parameter, each time minimizing the χ^2 with respect to all other NPAR-1 variable parameters, to numerically find the two values of the n-th parameter for which the minimum of χ^2 takes on the values FMIN+UP, where FMIN is the minimum of χ^2 with respect to all NPAR parameters. In order to make the procedure as fast as possible, MINOS uses the error matrix to predict the value of all parameters at the various sub-minima which it will have to find in the course of the calculation; if the problem is nearly linear, the predictions of MINOS will be nearly

exact, requiring very few iterations. An example of the output of MIGRAD is given in Fig. 15.

Finally, the program stops with the command EXIT, remembering at the user the χ^2/DOF value.

Figure 13: Example of input file

```
1  'dT0'        1.0e-4      1.0e-5
2  'mu'         1.0e-4      1.0e-5     -1.0     1.0
3  'yezh'       5           0.001       0.001   5.000
4  'uheat0'     0.          1.0e-5
5  'yB0'        0.          0.001
6  'history'     -10         0.001      -20.0    20.0
7  'nfi'        -1          0.001
8  'FI0'        1.0         0.001
9  'Te0'        1.0         0.001
10 'zstart'     10          0.001
11 'zend'       9.999       0.001
12 'omegab'     0.05        0.00001    0.01    1.0
13 'rh50'       1.00        0.001
14 'omegaNR'    1.00        0.001
15 'kn'         1.681322    0.001

FIX         3
FIX         4
FIX         5
FIX         6
FIX         7
FIX         8
FIX         9
FIX        10
FIX        11
FIX        12
FIX        13
FIX        14
FIX        15
ERROR DEF 4.
SIMPLEX
MINIMIZE
MINOS
HESSE
MATOUT
EXIT
```

Figure 14: Example of output file: we give the results of the routine MIGRAD for the computation of the minimum of the χ^2 and of the error matrix. Here FCN = χ^2.

```
**********
**   15 **MINIMIZE
**********
START MIGRAD MINIMIZATION.  STRATEGY 1.  CONVERGENCE WHEN EDM .LT. 0.40E-03

FCN=   260.6196     FROM MIGRAD    STATUS=INITIATE       8 CALLS       10 TOTAL
                    EDM= unknown      STRATEGY= 1      NO ERROR MATRIX

 EXT PARAMETER               CURRENT GUESS       STEP         FIRST
 NO.   NAME        VALUE            ERROR          SIZE      DERIVATIVE
  1   dT0         0.10000E-03   0.10000E-04   0.10000E-04   0.38589E+07
  2   mu          0.10000E-03   0.10000E-04   0.10000E-04   0.44111E+06
  3   yezh         5.0000          fixed
  4   uheat0      0.00000E+00      fixed
  5   yB0         0.00000E+00    constant
  6   istory      -10.000          fixed
  7   nfi         -1.0000          fixed
  8   FI0          1.0000          fixed
  9   Te0          1.0000          fixed
 10   zstart       10.000          fixed
 11   zend         9.9990          fixed
 12   omegab      0.50000E-01      fixed
 13   rh50         1.0000          fixed
 14   omegaNR      1.0000          fixed
 15   kn           1.6810          fixed
                               ERR DEF=  4.00

MIGRAD MINIMIZATION HAS CONVERGED.

MIGRAD WILL VERIFY CONVERGENCE AND ERROR MATRIX.
COVARIANCE MATRIX CALCULATED SUCCESSFULLY

FCN=   45.02554     FROM MIGRAD    STATUS=CONVERGED     30 CALLS       32 TOTAL
                    EDM=  0.50E-05    STRATEGY= 1      ERROR MATRIX ACCURATE

 EXT PARAMETER                                        STEP         FIRST
 NO.   NAME        VALUE            ERROR          SIZE      DERIVATIVE
  1   dT0        -0.69284E-06   0.16074E-04   0.25607E-07   -320.54
  2   mu          0.32603E-05   0.74528E-04   0.11874E-06   -80.453
  3   yezh         5.0000          fixed
  4   uheat0      0.00000E+00      fixed
  5   yB0         0.00000E+00    constant
  6   istory      -10.000          fixed
  7   nfi         -1.0000          fixed
  8   FI0          1.0000          fixed
  9   Te0          1.0000          fixed
 10   zstart       10.000          fixed
 11   zend         9.9990          fixed
 12   omegab      0.50000E-01      fixed
 13   rh50         1.0000          fixed
 14   omegaNR      1.0000          fixed
 15   kn           1.6810          fixed
                               ERR DEF=  4.00

EXTERNAL ERROR MATRIX.    NDIM=  50    NPAR=  2    ERR DEF=  4.00
 0.258E-09-0.434E-09
-0.434E-09 0.555E-08

PARAMETER  CORRELATION COEFFICIENTS
      NO.  GLOBAL     1     2
       1  0.36247  1.000-0.362
       2  0.36247 -0.362 1.000
```

Figure 15: Example of output file: we give the results of the routine MINOS for the computation of the errors. Here FCN = χ^2.

```
**********
**   16 **MINOS
**********

MINUIT TASK: 1 1 1 1 1 1 1

FCN=   45.02554     FROM MINOS     STATUS=SUCCESSFUL    24 CALLS       56 TOTAL
                    EDM=  0.50E-05    STRATEGY= 1      ERROR MATRIX ACCURATE

 EXT PARAMETER                  PARABOLIC         MINOS ERRORS
 NO.   NAME        VALUE          ERROR      NEGATIVE      POSITIVE
  1   dT0        -0.69284E-06   0.16074E-04  -0.16068E-04   0.16079E-04
  2   mu          0.32603E-05   0.74528E-04  -0.74487E-04   0.74566E-04
  3   yezh         5.0000         fixed
  4   uheat0      0.00000E+00     fixed
  5   yB0         0.00000E+00   constant
  6   istory      -10.000         fixed
  7   nfi         -1.0000         fixed
  8   FI0          1.0000         fixed
  9   Te0          1.0000         fixed
 10   zstart       10.000         fixed
 11   zend         9.9990         fixed
 12   omegab      0.50000E-01     fixed
 13   rh50         1.0000         fixed
 14   omegaNR      1.0000         fixed
 15   kn           1.6810         fixed
```

B FIGURES OF THE FITS OF THE AVAILABLE DATA

We report here the figures for the whole set of the fits to the available measures of the CMB absolute temperature.

Each figure shows three plots with the three different values of the cosmological parameter Ω_b; H_0 is set to 50 Km/s/Mpc.

The best fit values and the 95% CL limits on $\Delta\epsilon/\epsilon_i$ as well as the χ^2/DOF value corresponding to the best fit values are reported as functions of y_h. We report also in the plots the values of z_h corresponding to y_h as obtained by a simple power law approximation of eq. (2). See Tab. 8 for a more precise correspondence.

	$\hat{\Omega}_b$		
y_h	0.01	0.05	0.1
5.000	9.65×10^5	4.33×10^5	3.07×10^5
4.000	8.63×10^5	3.88×10^5	2.75×10^5
3.000	7.48×10^5	3.36×10^5	2.38×10^5
2.000	6.11×10^5	2.75×10^5	1.95×10^5
1.000	4.33×10^5	1.95×10^5	1.3×910^5
0.500	3.07×10^5	1.39×10^5	0.99×10^5
0.250	2.18×10^5	0.99×10^5	0.71×10^5
0.100	1.39×10^5	0.63×10^5	0.45×10^5
0.050	0.99×10^5	0.45×10^5	0.33×10^5
0.025	0.71×10^5	0.33×10^5	0.24×10^5
0.010	0.45×10^5	0.21×10^5	0.15×10^5

Table 8: Redshift corresponding to y_h for $\Omega = 1$, $H_0 = 50$ km/s/Mpc, $T_e/T_r = 1$, $T_0 = 2.725$ K and three massless neutrino species ($\kappa \simeq 1.68$),

Figure 16: Values of the fractional energy injected in the radiation field as obtained from the fit to the FIRAS data alone. The solid line is the best-fit, the dashed lines are the upper and the lower limits at 95% CL.

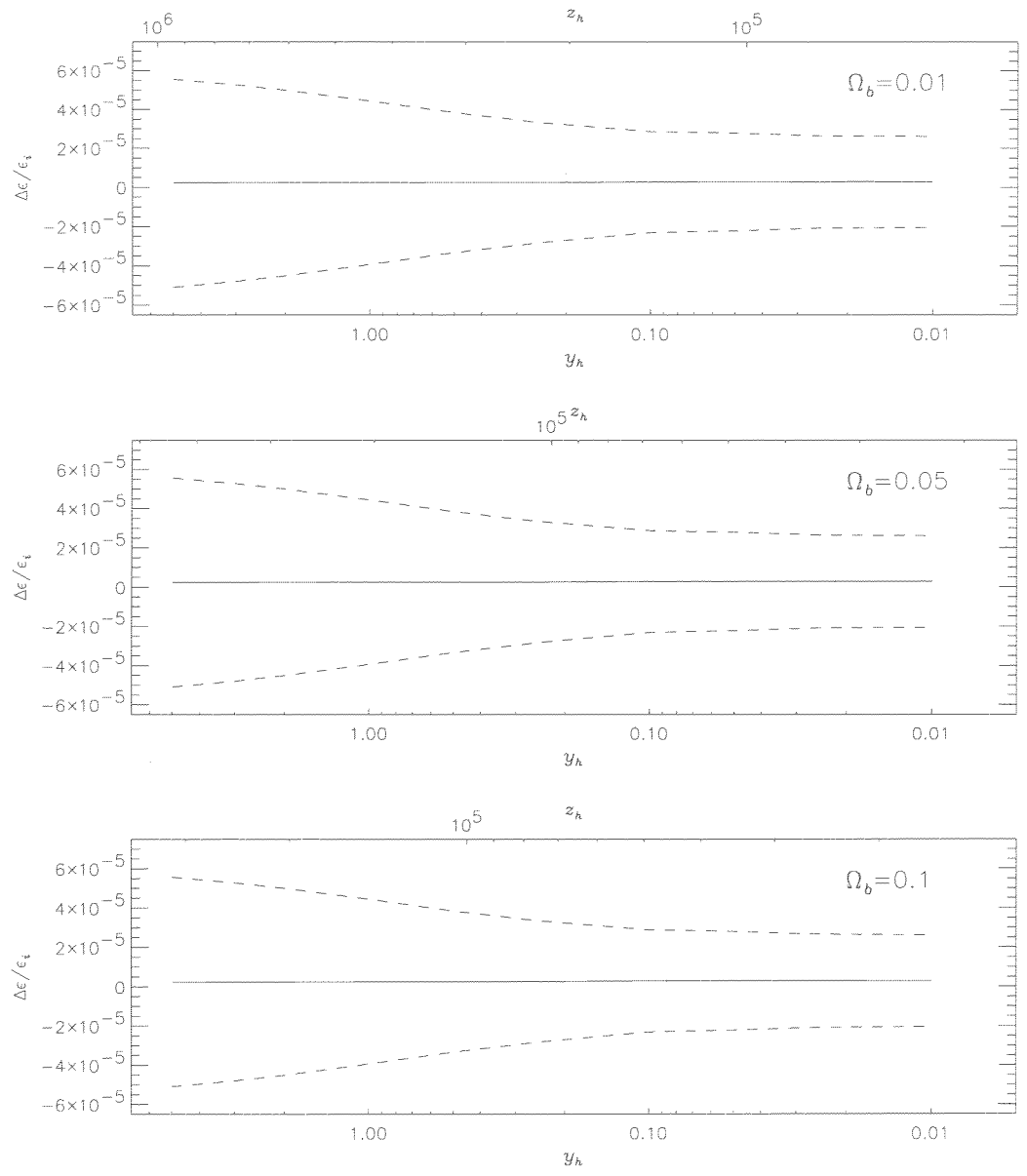

Figure 17: Values of χ^2/DOF for the fit to the FIRAS data alone. We fit 47 data with 2 parameters: T_0 and $\Delta\epsilon/\epsilon_i$.

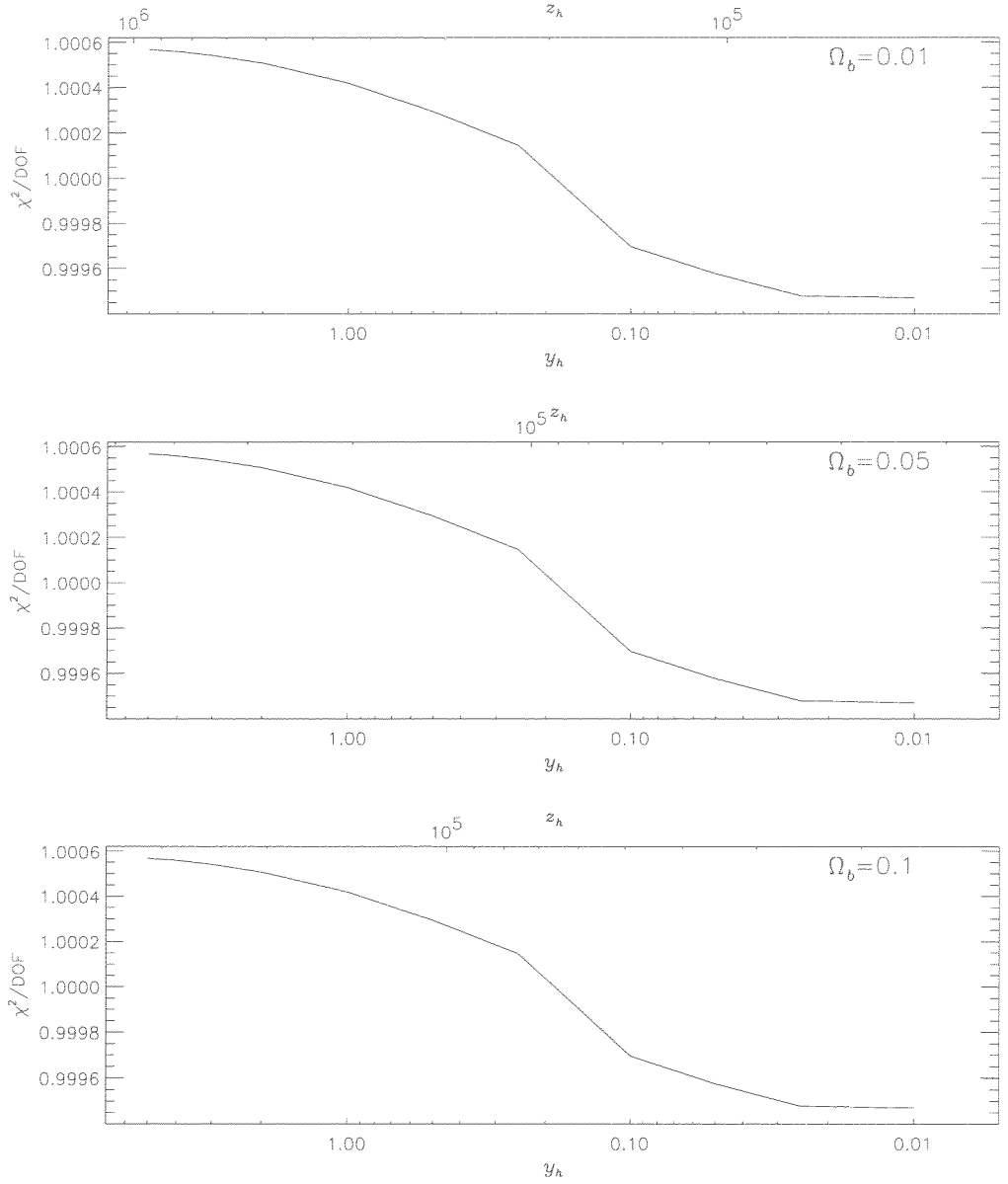

Figure 18: Values of the fractional energy injected in the radiation field as obtained from the fit of the recent data jointed to the FIRAS data calibrated at 2.725 K. The solid line is the best-fit, the dashed lines are the upper and the lower limits at 95% CL.

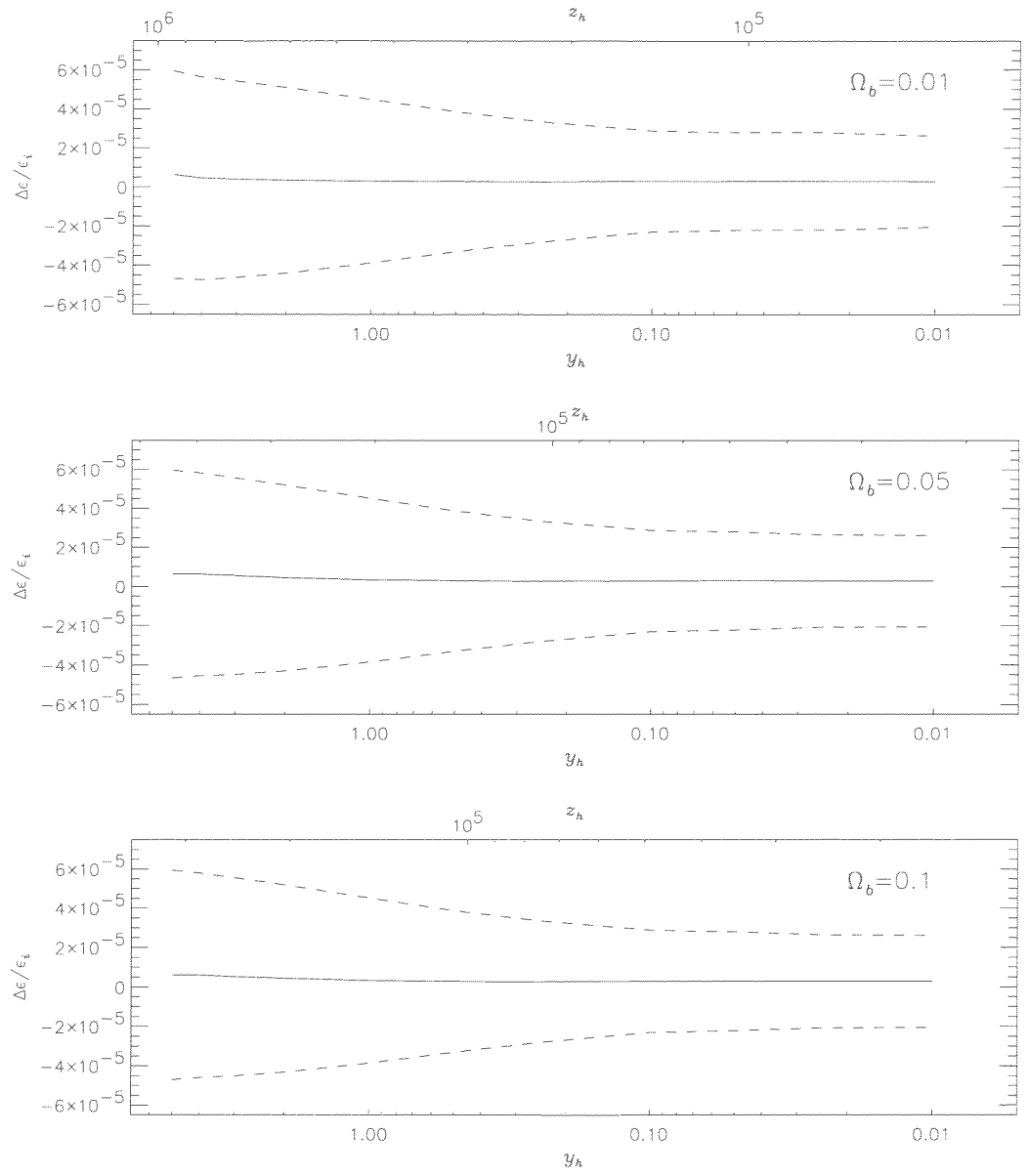

Figure 19: Values of χ^2/DOF for the fit to the recent data jointed to the FIRAS data calibrated at 2.725 K. We fit 64 data with 2 parameters: T_0 and $\Delta\epsilon/\epsilon_i$.

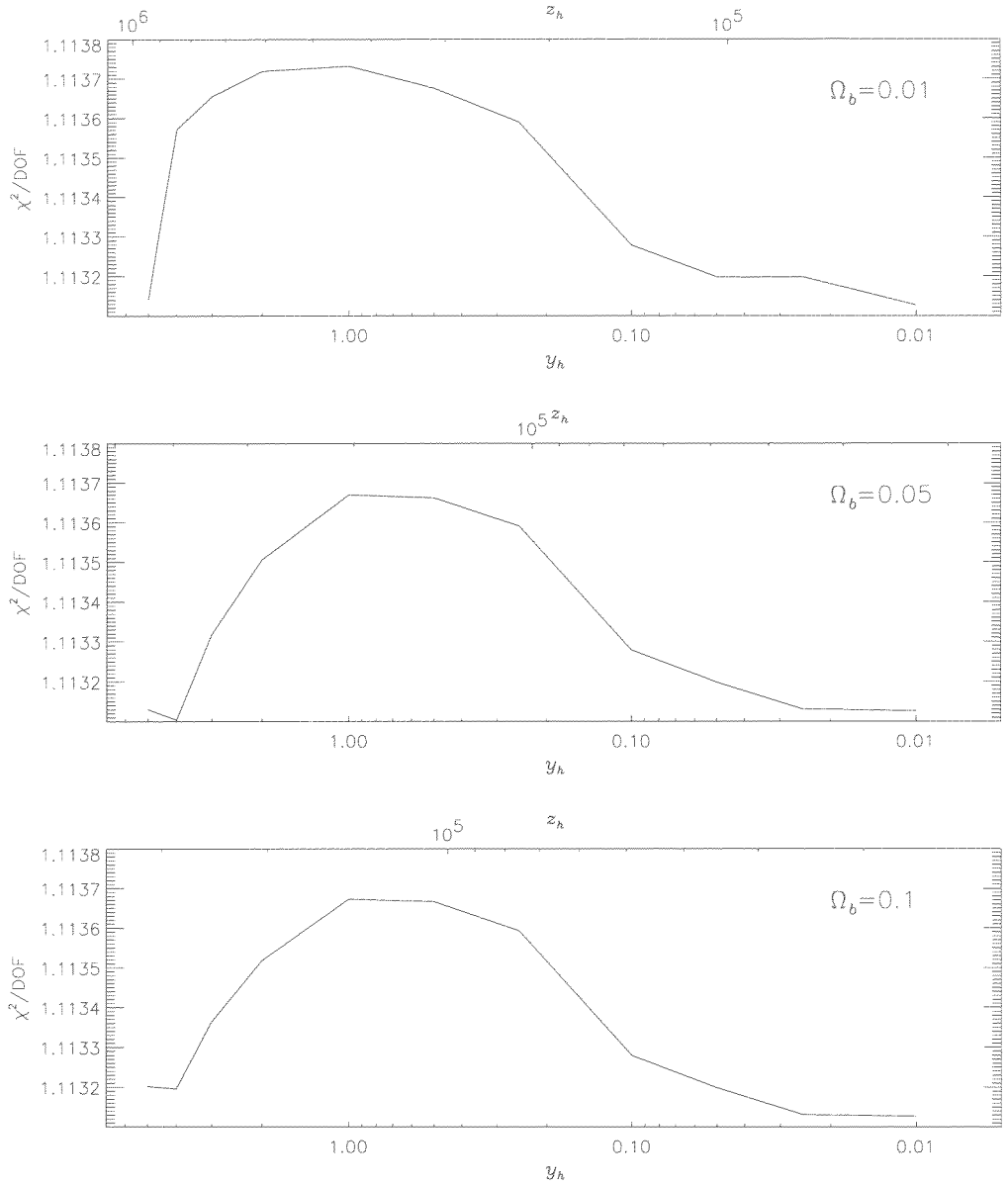

Figure 20: The same as in Fig. 18 but for the FIRAS data calibrated at 2.723 K.

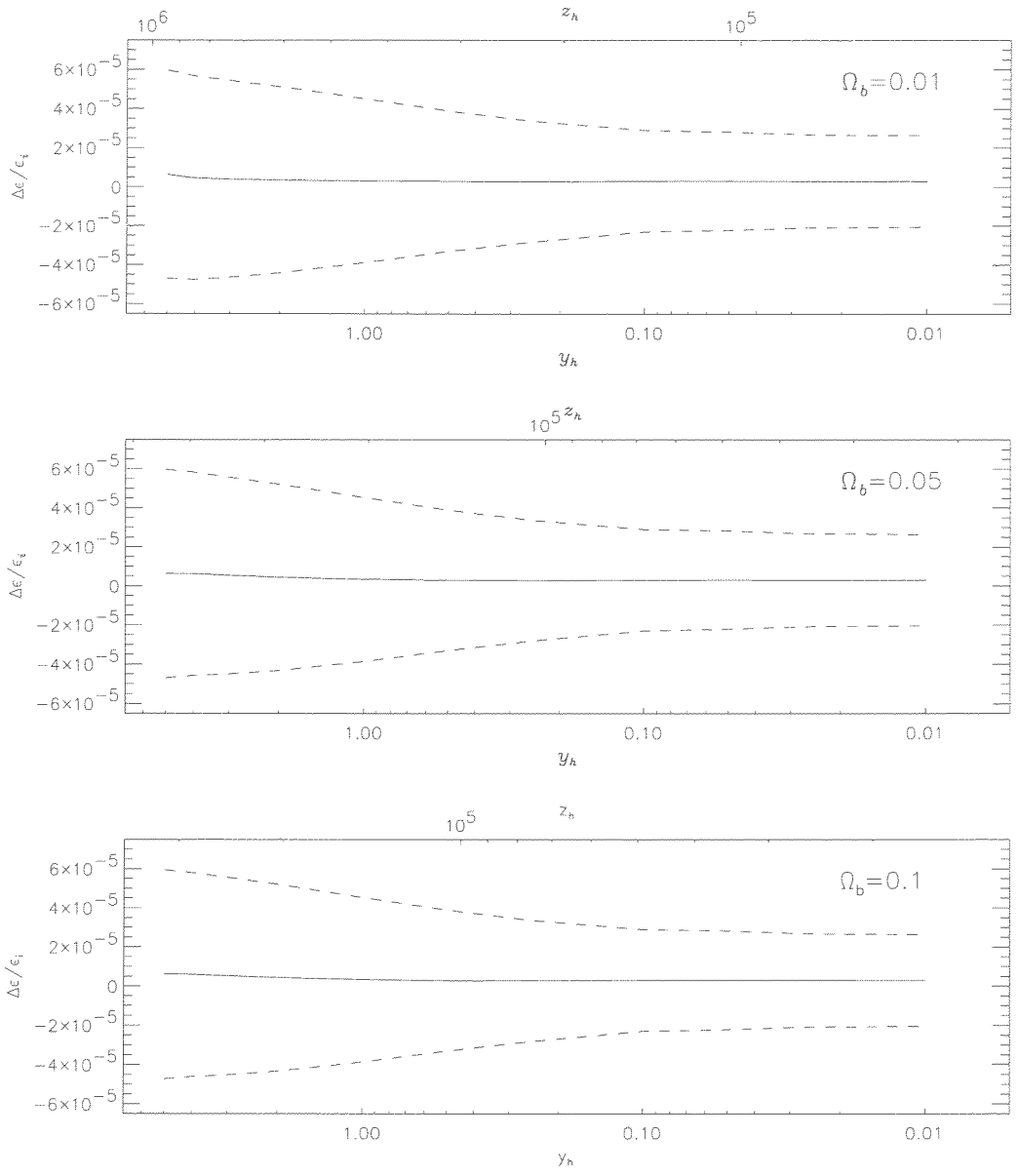

Figure 21: The same as in Fig. 19 but for the FIRAS data calibrated at 2.723 K.

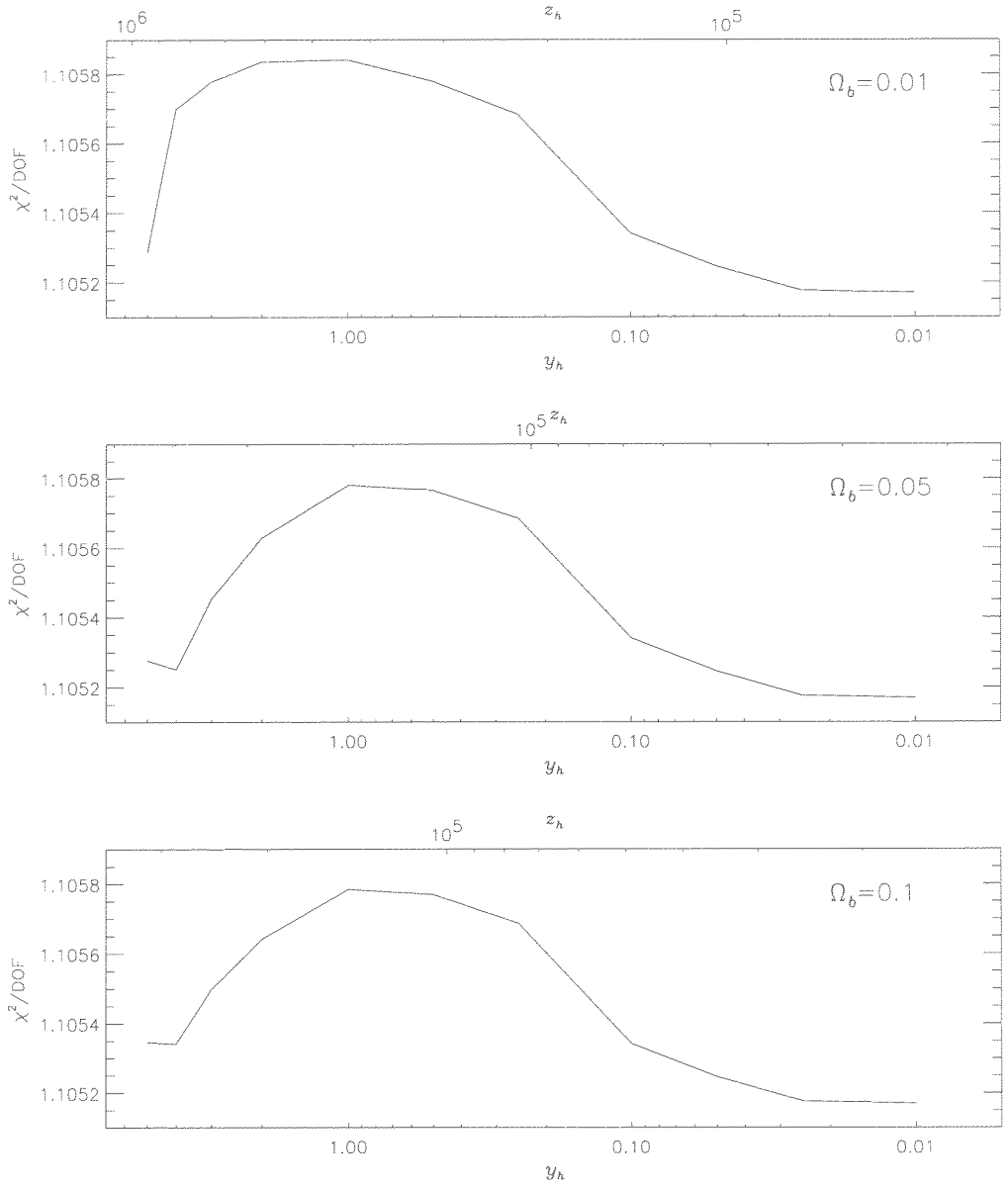

Figure 22: The same as in Fig. 18 but for the FIRAS data calibrated at 2.727 K.

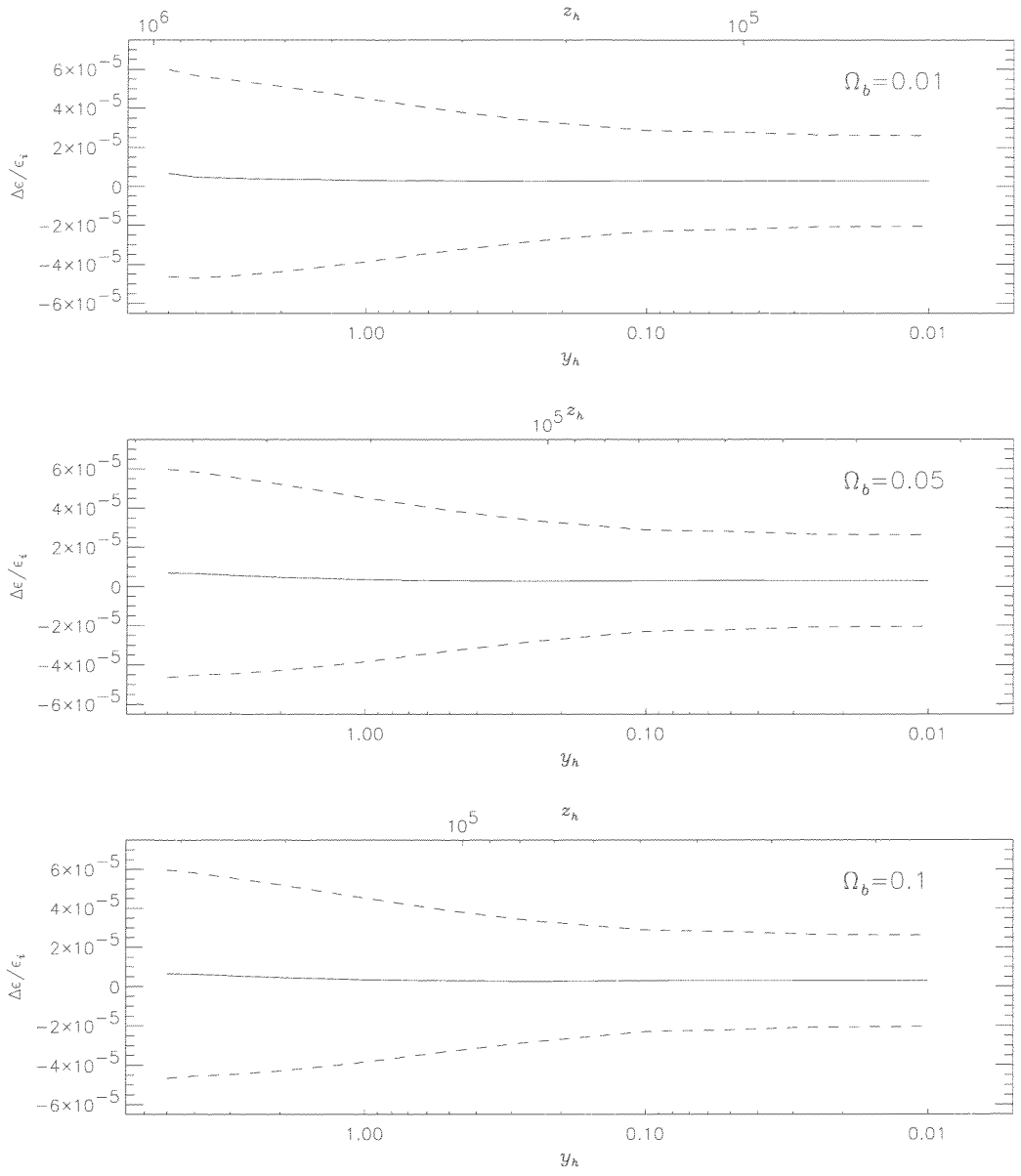

Figure 23: The same as in Fig. 17 but for the FIRAS data calibrated at 2.727 K.

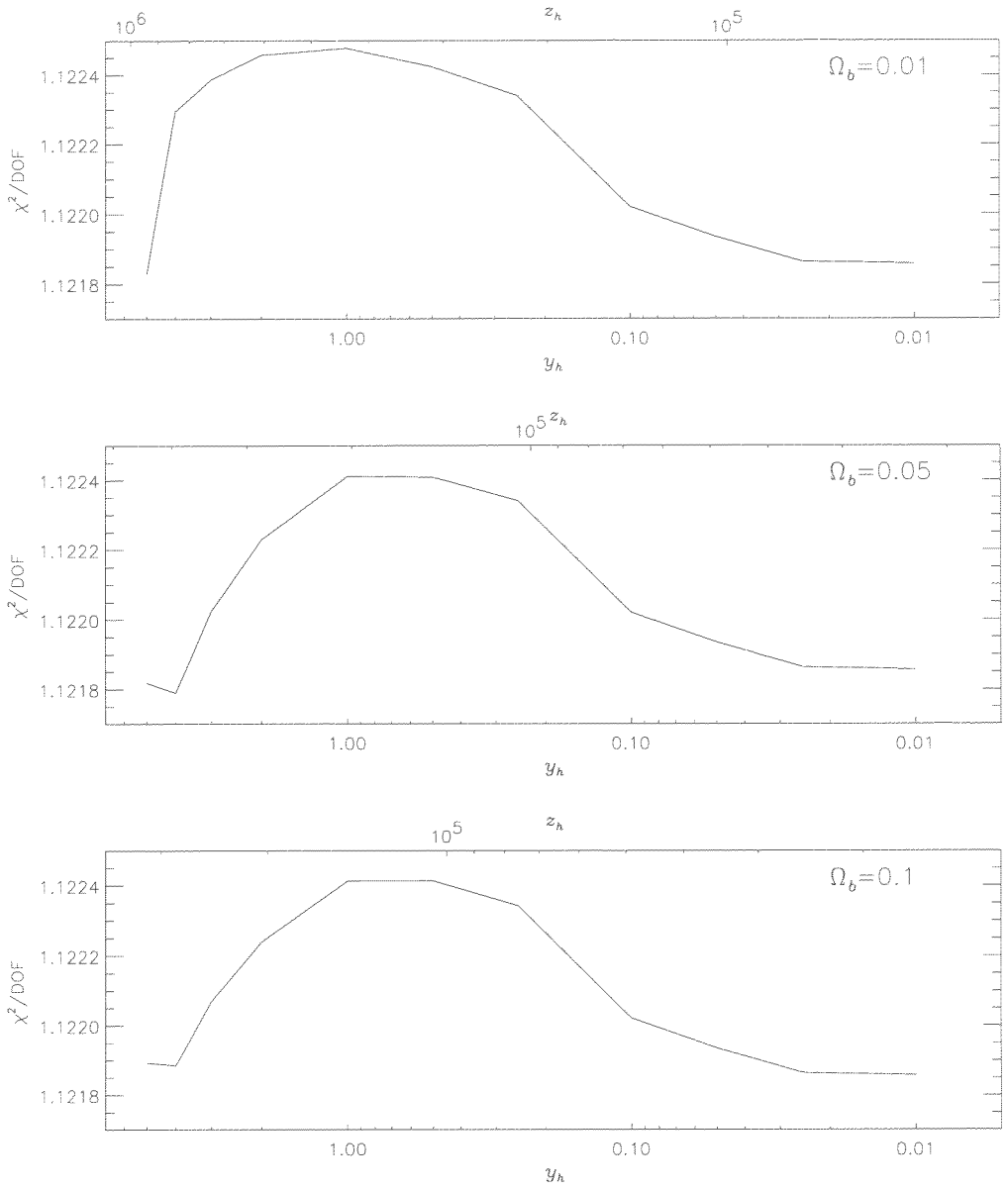

Figure 24: Results of the fit on the energy injected at any given value of y_h and relative upper and lower limits at 95% CL by allowing also for an energy dissipation at low z. We used here the recent data jointed to the FIRAS data calibrated at 2.725 K.

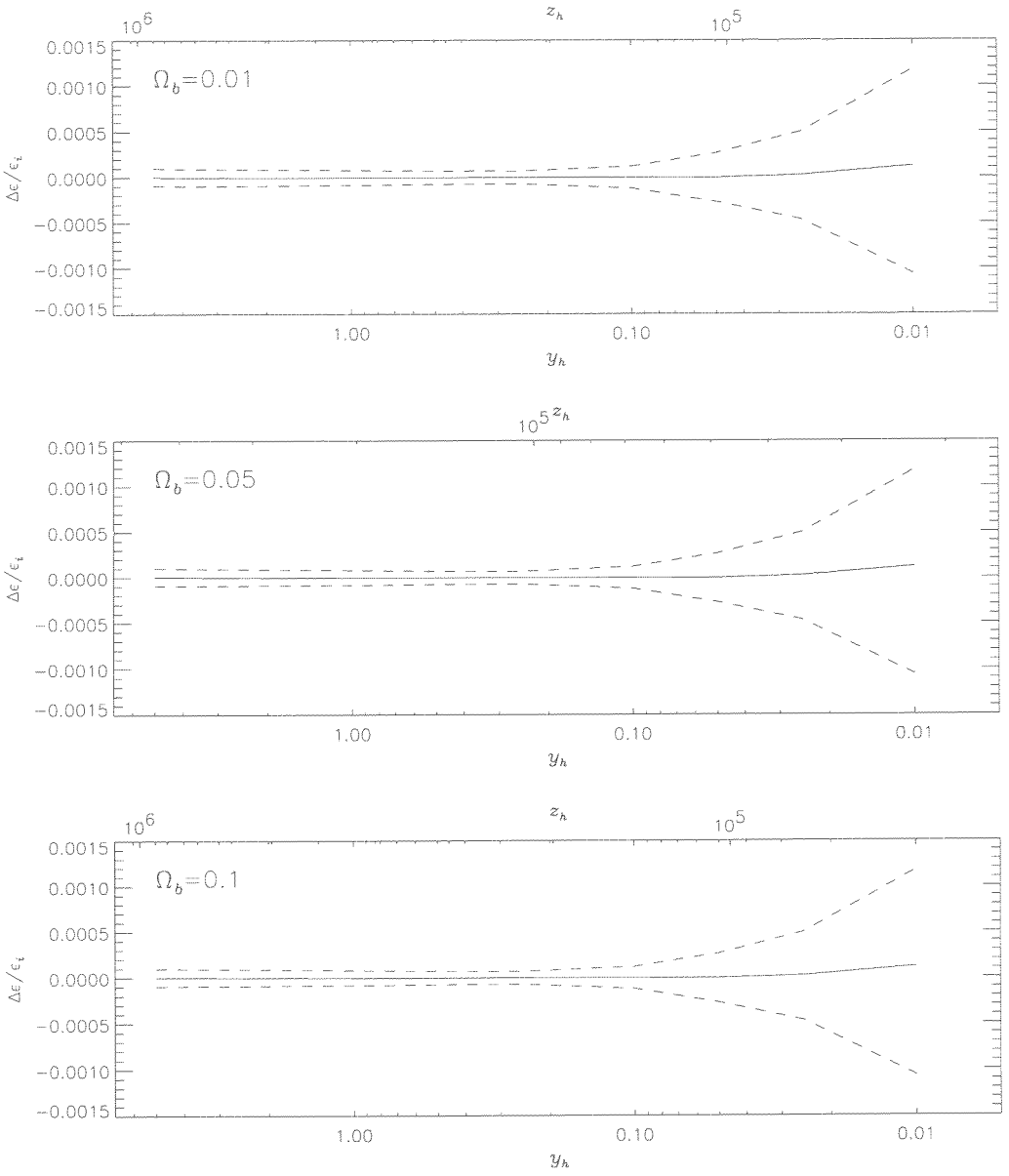

Figure 25: Results of the fit on the energy injected at low z and relative upper and lower limits at 95% CL if the spectrum is just distorted at any given value of y_h. We used here the recent data and the FIRAS data calibrated at 2.725 K.

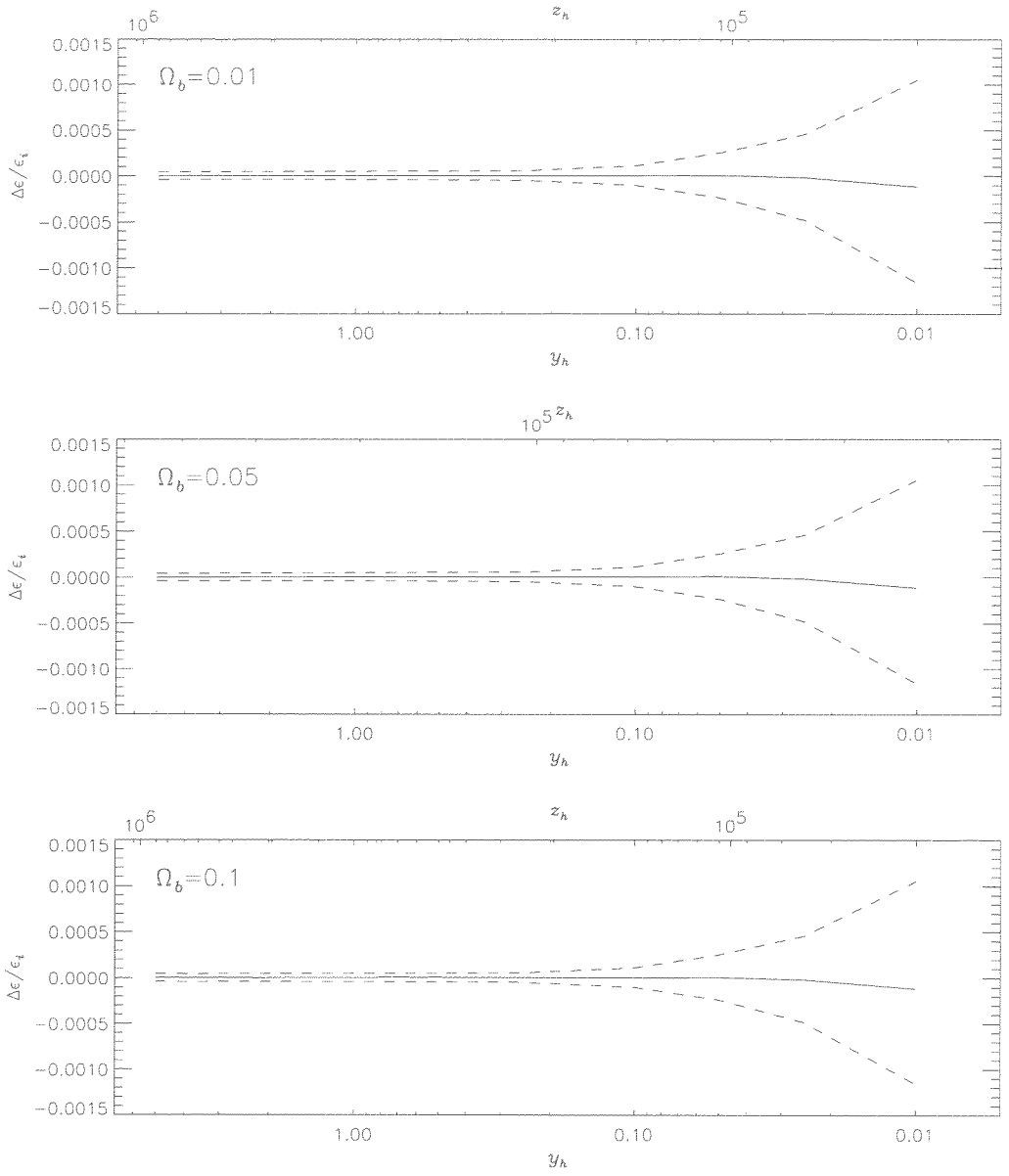

Figure 26: Values of the χ^2/DOF for the fit to the recent data jointed to the FIRAS data calibrated at 2.725 K. We fit 64 data with 3 parameters: T_0 and two values of $\Delta\epsilon/\epsilon_i$ corresponding to two dissipation processes at different epochs.

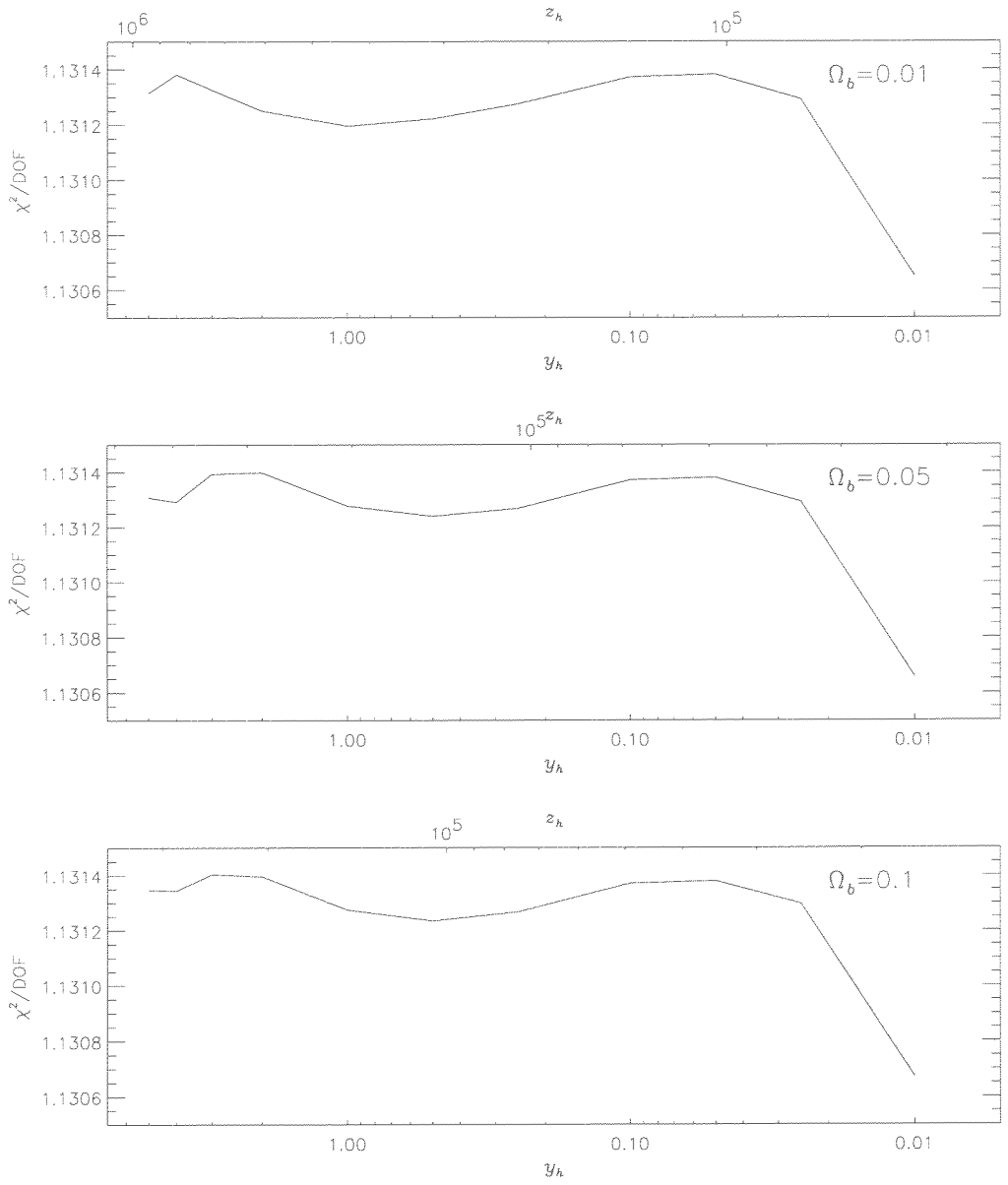

Figure 27: The same as in Fig. 24 but for the FIRAS data calibrated at 2.723 K.

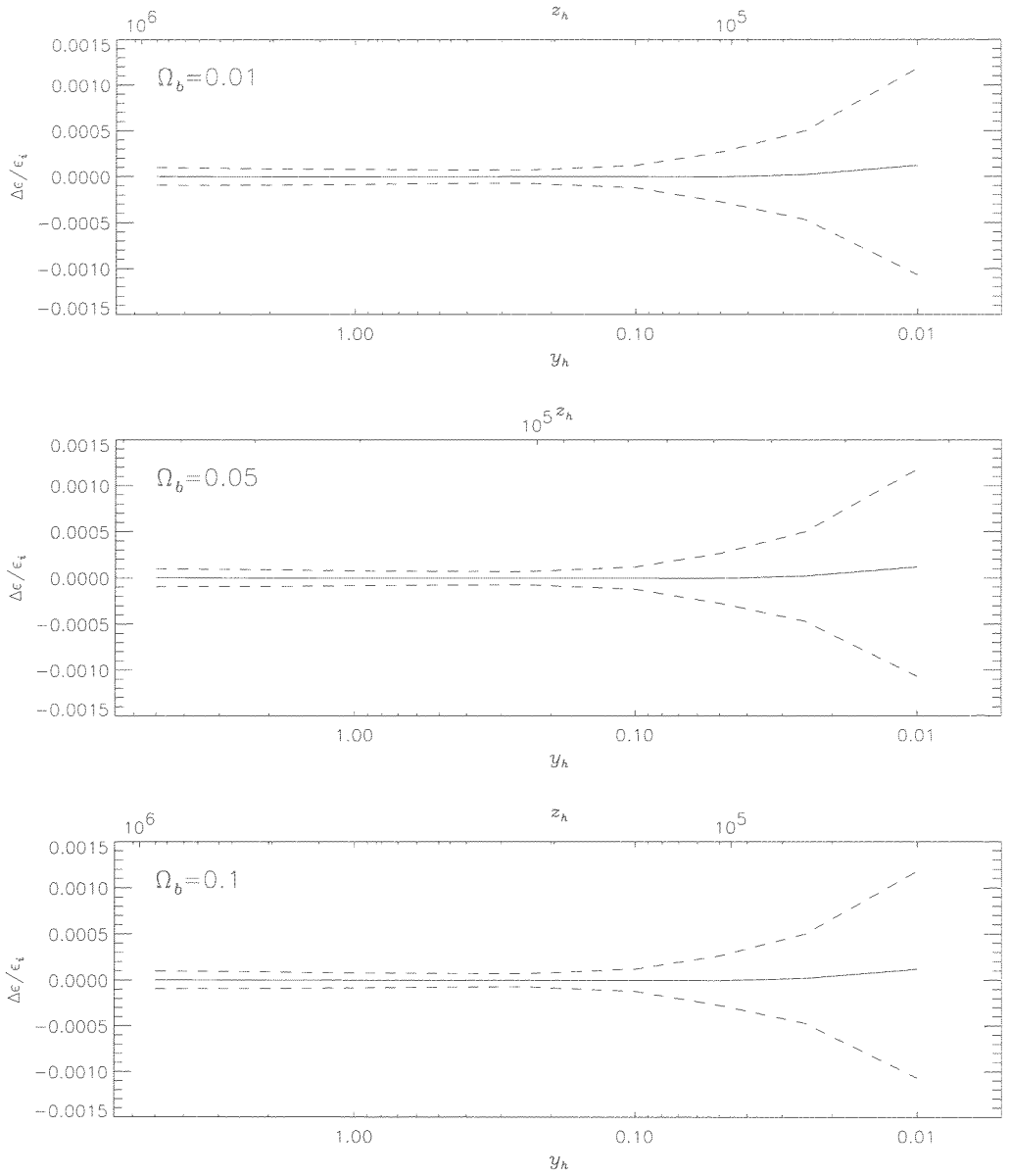

Figure 28: The same as in Fig. 25 but for the FIRAS data calibrated at 2.723 K.

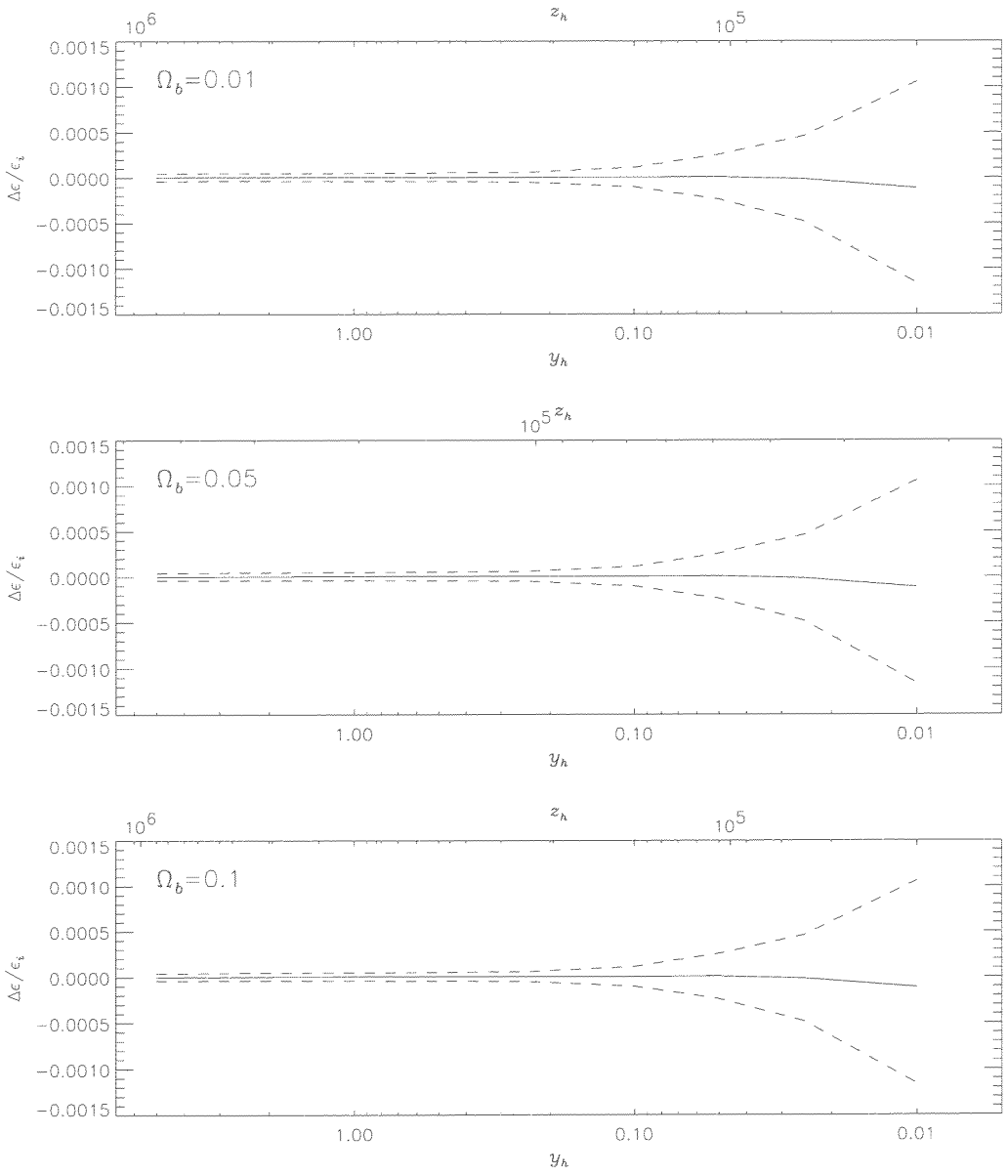

Figure 29: The same as in Fig. 26 but for the FIRAS data calibrated at 2.723 K.

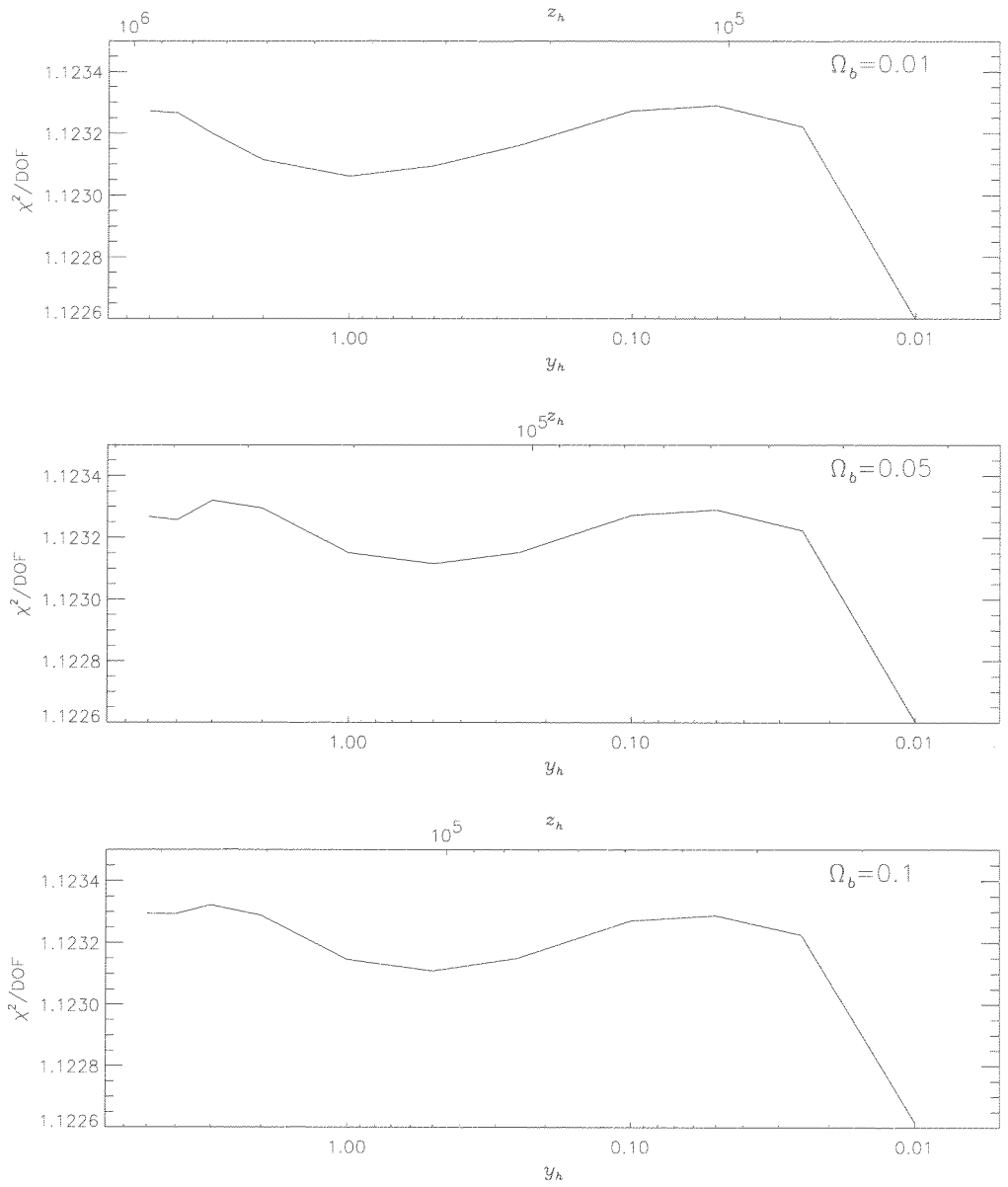

Figure 30: The same as in Fig. 24 but for the FIRAS data calibrated at 2.727 K.

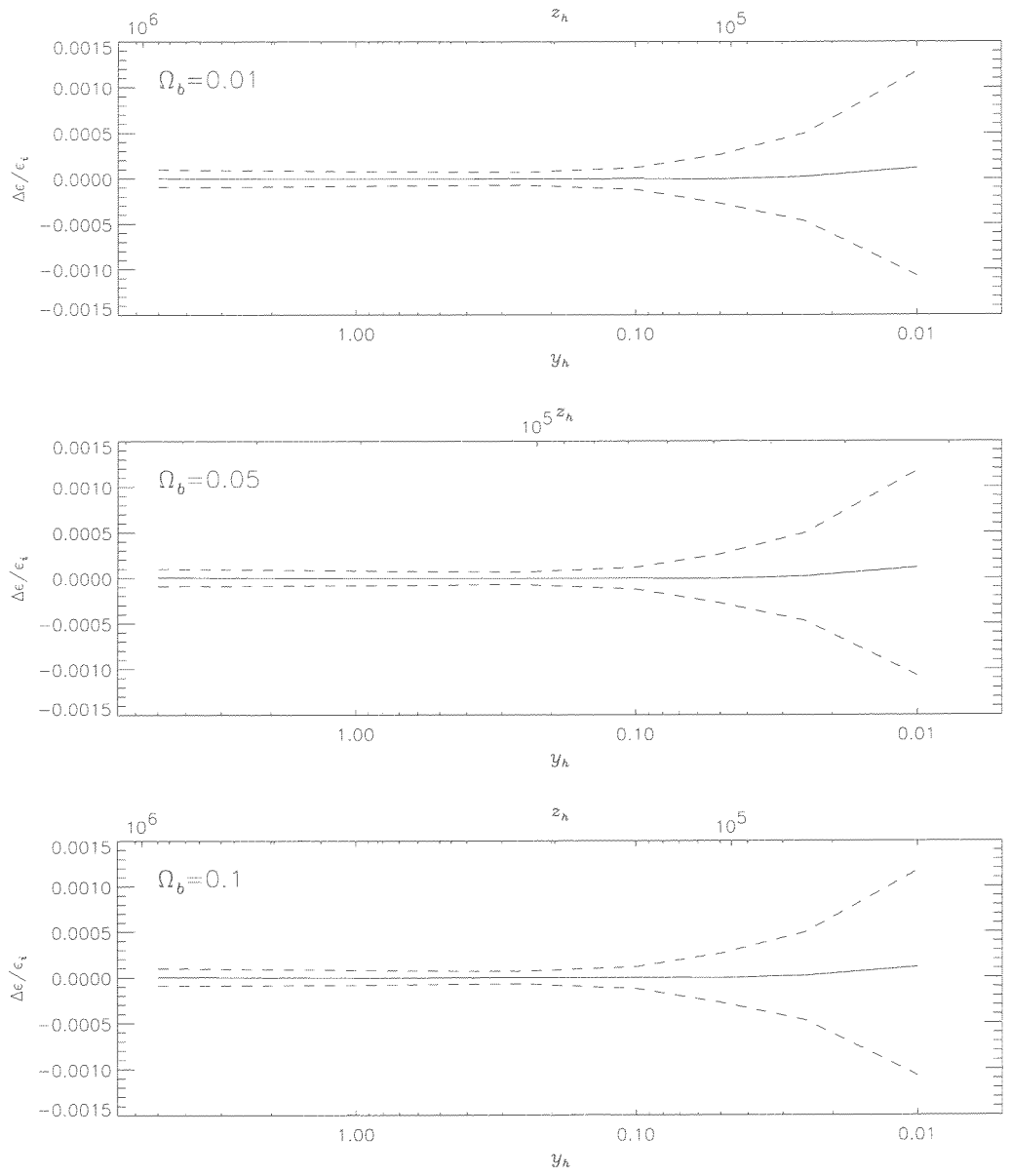

Figure 31: The same as in Fig. 25 but for the FIRAS data calibrated at 2.727 K.

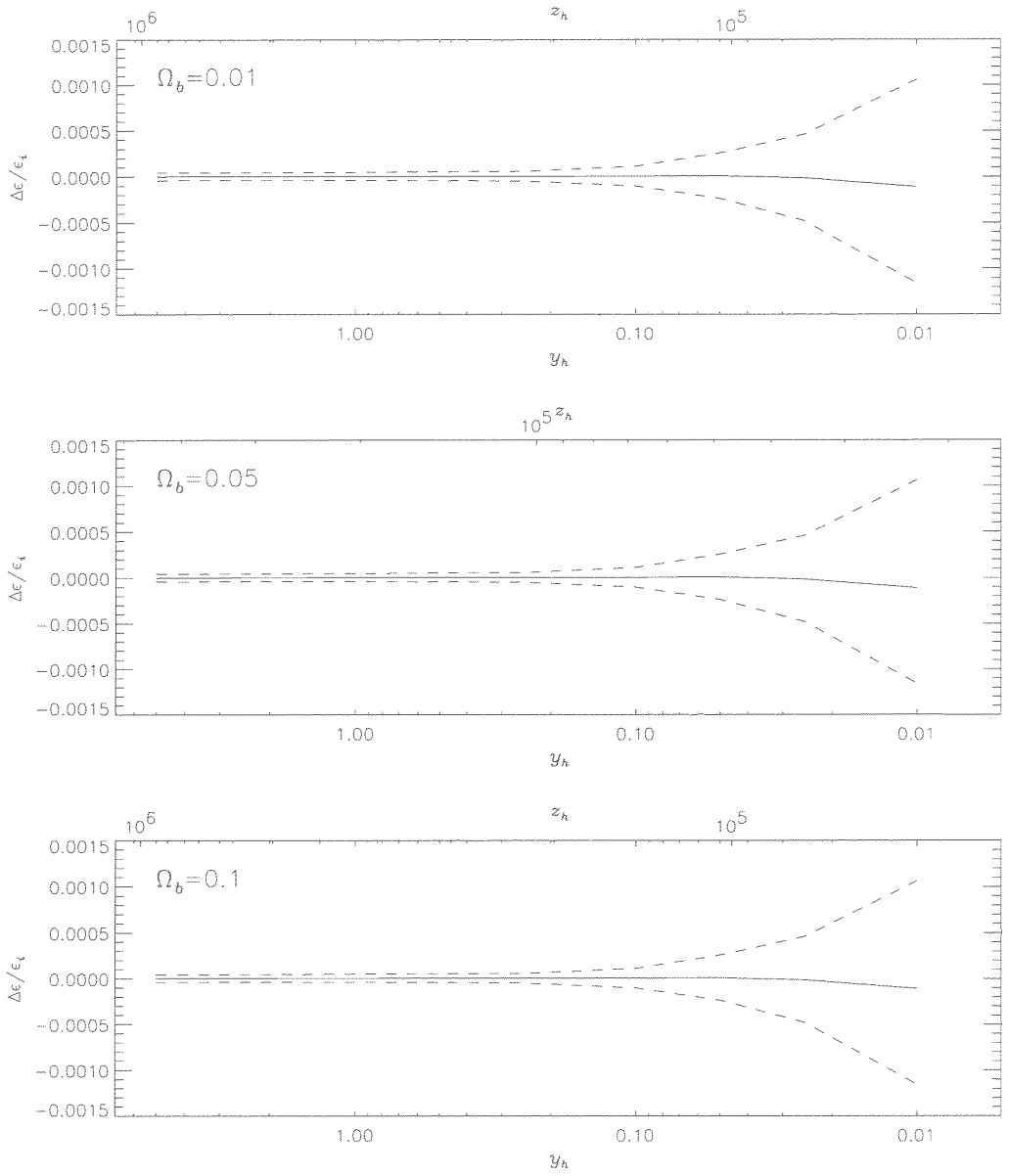

Figure 32: The same as in Fig. 26 but for the FIRAS data calibrated at 2.727 K.

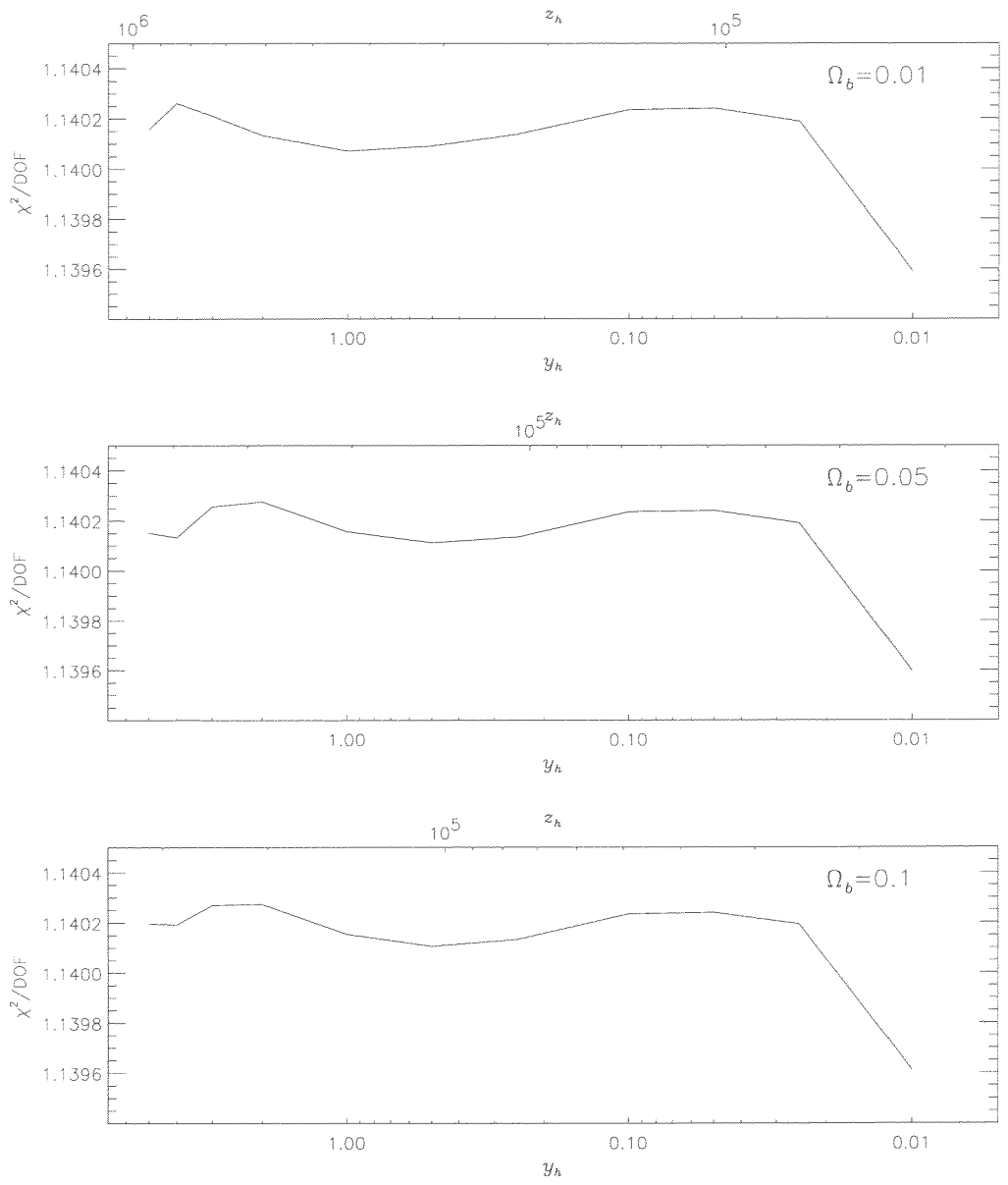

References

[1] Bensadoun M. et al. 1993, ApJ, 409, 1

[2] Bersanelli M. et al. 1989, ApJ, 339, 632

[3] Bersanelli M. et al. 1994, ApJ, 424, 517

[4] Burigana C. et al. 1991a, A&A, 246, 59

[5] Burigana C. et al. 1991b, ApJ, 379, 1

[6] Burigana C. et al. 1995, A&A, 303, 323

[7] Danese L., Burigana C. 1993, in: "Present and Future of the Cosmic Microwave Background", Lecture in Physics, Vol. 429, eds. J.L. Sanz, E. Martinez-Gonzales, L. Cayon, Springer Verlag, Heidelberg (FRG), p. 28

[8] Danese L., De Zotti G. 1977, Riv. Nuovo Cimento, 7, 277

[9] De Amici G. et al. 1985, ApJ, 298, 710

[10] De Amici G. et al. 1991, ApJ, 381, 341

[11] Fixsen D.J. et al. 1996, ApJ, 473, 576

[12] Johnson D.G., Wilkinson D.T. 1987, ApJL, 313, L1

[13] Kogut A. et al. 1988, ApJ, 325, 1

[14] Kogut A. et al. 1990, ApJ, 355, 102

[15] Kompaneets A.S. 1956, Zh. Eksp. Teor. Fiz., 31, 876 [Sov. Phys. JEPT, 4, 730, (1957)]

[16] Levin S.M. et al. 1988, ApJ, 334, 14

[17] Levin S.M. et al. 1992, ApJ, 396, 3

[18] Mandolesi N. et al. 1986, ApJ, 310, 561

[19] Mather J.C. et al. 1990, ApJ, 354, L37

[20] Mather J.C. et al. 1994, ApJ, 420, 439

[21] Mather J.C. et al. 1999, ApJ, 512, 511

[22] Nordberg H.P., Smoot G.F. 1998, Preprint astro-ph/9805123

[23] Salvaterra R., Burigana C. 2000, Int. Rep. ITeSRE/CNR 270/2000

[24] Schuster et al. UC Berkeley PhD Thesis

[25] Sironi G. et al. 1990, ApJ, 357, 301

[26] Sironi G. et al. 1991, ApJ, 378, 550

[27] Staggs S. et al. 1996a, ApJ, 458, 407

[28] Staggs S. et al. 1996b, ApJ, 473, L1

[29] Zeldovich Ya.B., Sunyaev R.A. 1969, Ap&SS, 4, 301

[30] Zeldovich Ya.B., Illarionov A.F., Sunyaev R.A. 1972, Zh. Eksp. Teor. Fiz., 62, 1216 [Sov. Phys. JEPT, 35, 643]